

### **Details of the research work for the Sun Pharma Research Award**

**Publication #1:** Goel S, Bhatia V, Kundu S, Biswas T, Carskadon S, Gupta N, Asim M, Morrissey C, Palanisamy N, **Ateeq B\***. Transcriptional network involving ERG and AR orchestrates Distal-Less Homeobox-1 mediated prostate cancer progression. *Nature Communications*. 2021 Sep 7;12(1):5325. doi: 10.1038/s41467-021-25623-2. **Impact Factor: 14.919.**

The *Distal-less homeobox (DLX)* genes belong to the homeobox containing family of transcription factors (TFs), which are structural homologs of *Drosophila Distal-less (Dll)*. *DLX1* being a member of the *DLX* family plays an essential role in the development of craniofacial features, jaw, and GABAergic (gamma-aminobutyric acid) interneuron<sup>1</sup>. Dereglulation of homeobox genes has been linked to several human malignancies including prostate<sup>2</sup>. In hematopoietic cells, *DLX1* impedes downstream TGF- $\beta$ -mediated signaling pathways by interacting with Smad4<sup>3</sup>. In PCa, *DLX1* is known to functionally interact with  $\beta$ -catenin and regulate downstream  $\beta$ -catenin/TCF4 signaling pathway<sup>4</sup>. Furthermore, *DLX1* has been validated as a PCa biomarker across clinically independent cancer cohorts, wherein *DLX1* and *HOXC6* accurately predict high-grade disease<sup>5</sup>. However, the underlying regulatory mechanism that drives *DLX1* upregulation and its functional role in PCa progression remain poorly understood.

Here, we uncover the molecular mechanisms underlying upregulation of *DLX1* in PCa and reveal oncogenic functions associated with it. Our data identify *DLX1*-mediated downstream biological processes that operate in PCa tumorigenesis and show its oncogenic role in disease progression and metastasis. We also demonstrate the role of ERG, AR and FOXA1 as key transcriptional regulators involved in *DLX1* overexpression in PCa. Lastly, we show that disrupting ERG/AR transcriptional circuitry with BET inhibitor (BETi) or in combination with anti-androgen could attenuate *DLX1*-mediated tumorigenesis. Collectively, this study highlights the importance of *DLX1* as an effective therapeutic target in PCa patients irrespective of *TMPRSS2-ERG* fusion status.

#### ***DLX1 imparts oncogenic properties and promotes PCa progression***

Using publicly available clinical genomics data repository viz. The Cancer Genome Atlas Prostate Adenocarcinoma (TCGA-PRAD) dataset, we have shown that higher expression of *DLX1* in patients with primary PCa compared to matched normal tissue (Fig. 1a). In agreement with this, patients with higher *DLX1* expression (*DLX1*<sup>Hi</sup>) experienced poor survival probability compared to those with lower *DLX1* expression (*DLX1*<sup>Lo</sup>) (Fig. 1c). Interestingly, a significant increase in cell proliferation in *DLX1* overexpressing RWPE cells (RWPE1-*DLX1*) compared to control was observed (Fig. 1e). Similarly, *DLX1* overexpression markedly increased foci forming ability and migratory properties of RWPE1 cells (Fig. 1f-g). Three independent *DLX1* knockout (KO) *DLX1*-KO clones, namely 22RV1-*DLX1*-KO (C-1, C-2 and C-3) showing loss of *DLX1* expression both at transcript and protein levels were selected to determine any phenotypic changes in these genetically engineered lines. Notably, a marked reduction in proliferation rates of 22RV1-*DLX1*-KO cells was observed compared to control (Fig. 1h). Similarly, a significant reduction (~60%) in the cell migratory and foci forming properties, and anchorage-independent growth was observed in 22RV1-*DLX1*-KO cells compared to control cells (Fig. 1i-j). Our microarray-based global gene expression profiling of 22RV1-*DLX1*-KO and 22RV1-SCR cells, showed genes involved in proliferation and migration of cells, and stem-cell population maintenance were negatively enriched in 22RV1-*DLX1*-KO cells, while genes associated with cell cycle regulation and antigen processing and presentation were

upregulated (Fig. 1k-m). Taken together, our findings implicate the critical role of DLX1 in imparting oncogenic properties to prostate cells.

**Figure 1**

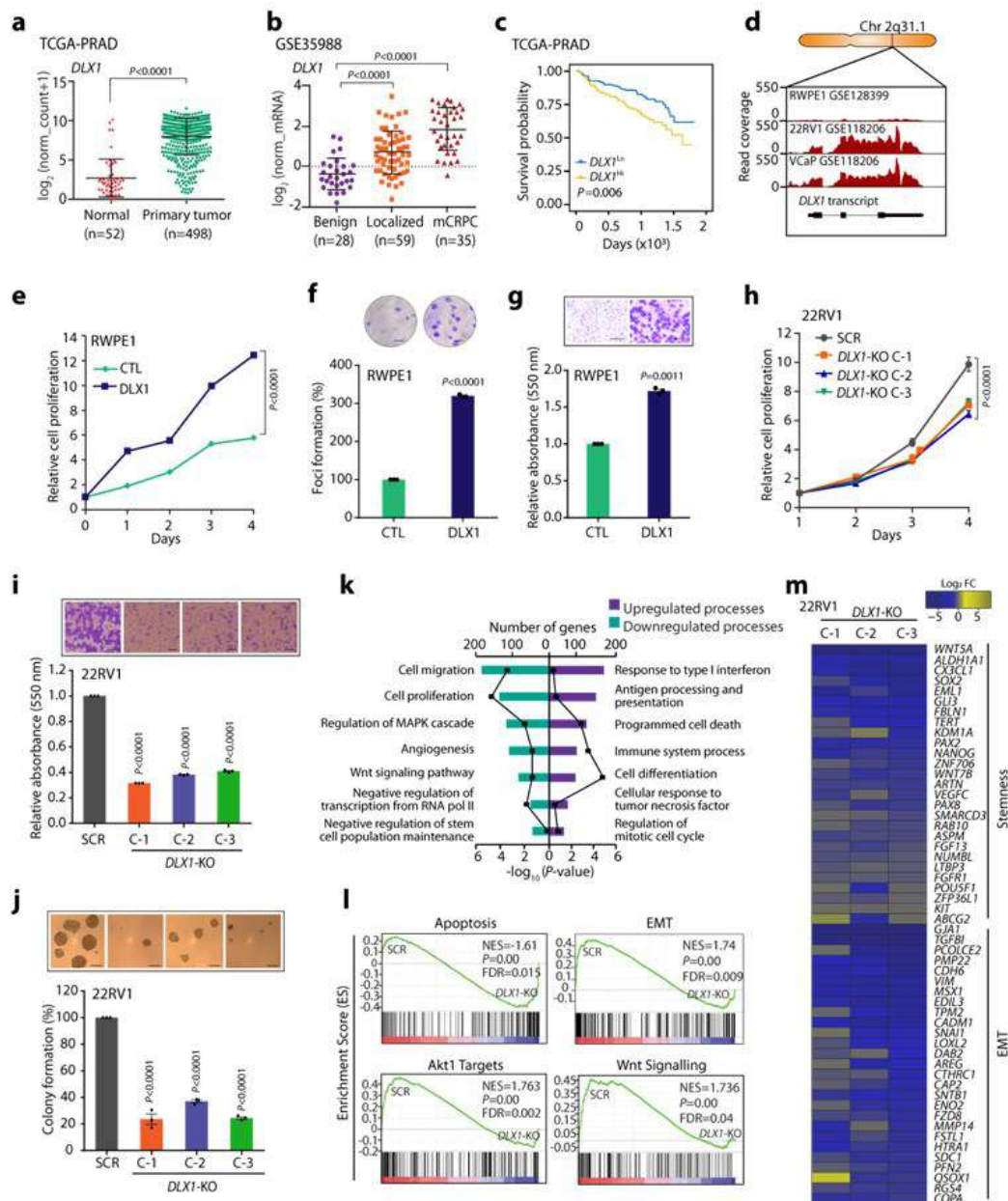


**Figure 1. High DLX1 expression associates with poor prostate cancer prognosis and promotes disease progression.** **a** Dot plot showing *DLX1* expression in PCa patients (n=498) and matched normal (n=52) in TCGA-PRAD RNA-Seq dataset, data represents log<sub>2</sub> (norm\_count+1), centre depicts mean  $\pm$  (standard deviation) SD ( $P < 0.0001$ ). **b** Dot plot of *DLX1* expression using microarray profiling data (GSE35988) comprising benign (n=28), localised (n=59), and mCRPC (n=35) patient specimens, data represents log<sub>2</sub> (norm\_mRNA), centre depicts mean  $\pm$  SD ( $P < 0.0001$ ). **c** Kaplan-Meier plot showing survival probability in TCGA-PRAD (n=498) dataset categorized in high *DLX1* (*DLX1*<sup>Hi</sup>) and low *DLX1* (*DLX1*<sup>Lo</sup>) expression. **d** RNA-Seq data showing *DLX1* transcript read counts in publicly available datasets (GSE128399 and GSE118206). **e** Cell proliferation assay using isogenic RWPE1 cells overexpressing *DLX1* at indicated time-points ( $P < 0.0001$ ). **f** Foci formation assay using same cells as **e** ( $P < 0.0001$ ). **g** Boyden Chamber Matrigel migration assay using same cells as **e** ( $P < 0.0001$ ). Representative images for panels **f** (scale bar 500 $\mu$ m) and **g** (scale bar 100 $\mu$ m) are shown as inset. **h** Cell proliferation assay using 22RV1-*DLX1*-KO (C-1, C-2 and C-3 are independent clones) and control cells at indicated time-points ( $P < 0.0001$ ). **i** Boyden Chamber Matrigel migration assay using same cells as **h** ( $P < 0.0001$ ). **j** Anchorage-independent soft agar assay using same cells as **h** ( $P < 0.0001$ ). Representative images for panels **i** and **j** are shown as inset (scale bar 100 $\mu$ m). **k** DAVID analysis showing upregulated (right) and downregulated (left) biological processes in 22RV1-*DLX1*-KO against control cells. Bars represent the  $-\log_{10}(P\text{-value})$  and the frequency polygon (black line) denotes number of genes. **l** Same as **k**, except Gene Set Enrichment Analysis (GSEA) plots representing deregulated pathways. **m** Heatmap displaying genes downregulated involved in cancer stemness and EMT in 22RV1-*DLX1*-KO cells compared to control. Data shown from three biological independent samples (n=3).

**DLX1 elicits biological processes involved in cancer progression.** We observed reduced expression of two archetypal markers of the mesenchymal phenotype, namely Vimentin and Snail, with increased E-cadherin expression, an epithelial marker in *DLX1*-KO cells (Fig. 2a-b). Consistent with the GSEA data, an increased apoptosis marked by Caspase 3 activation and cleaved Poly-(ADP-ribose) polymerase (PARP) in *DLX1*-KO cells along with decrease in the levels of anti-apoptotic Bcl-xL was observed (Fig. 2c-d). Next, our flow-cytometry based cell cycle analysis revealed an increase in the percentage of cells arrested in the S-phase with a concomitant decrease in the G2/M phase cells in *DLX1*-KO compared to control (Fig. 2e). Similarly, small interfering RNA (siRNA)-mediated transient knockdown of *DLX1* in VCaP cells resulted in cell cycle arrest (Fig. 2e). In agreement with the microarray data, *DLX1*-KO cells exhibit decreased expression of established stem cell markers (Fig. 2f).

Figure 2

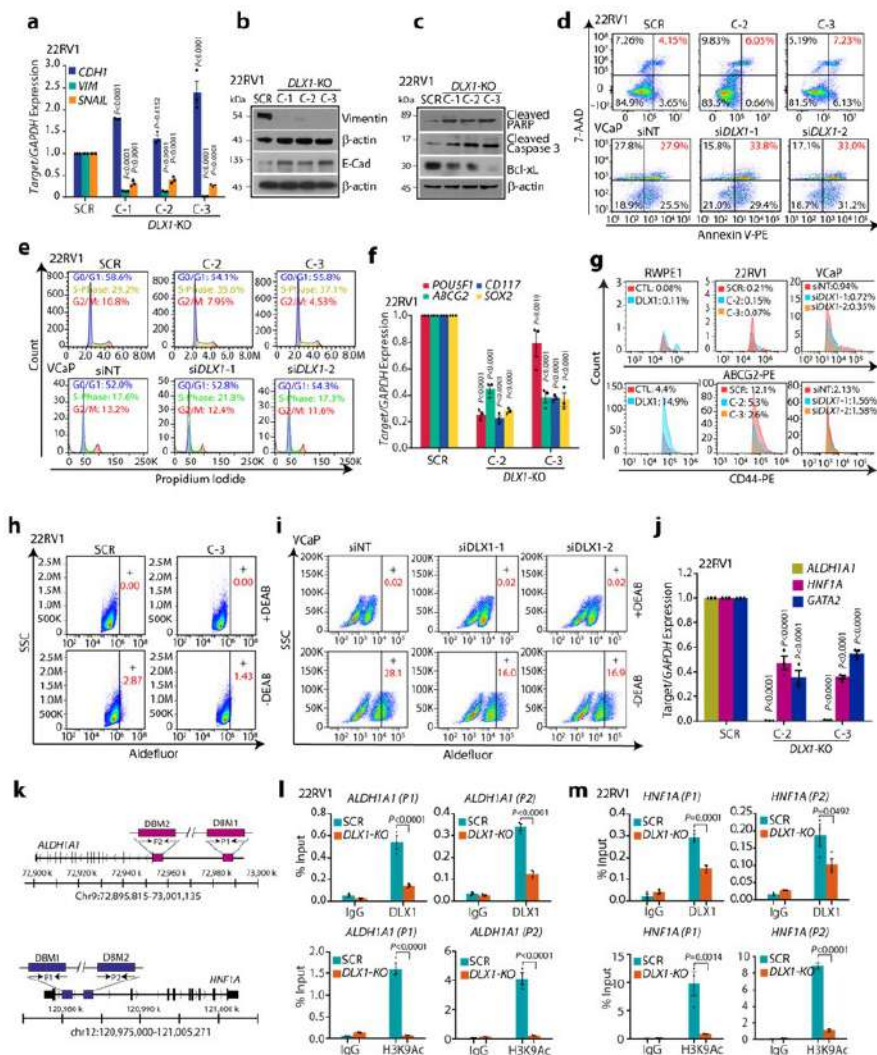


**Figure 2. Genetic ablation of *DLX1* inhibits oncogenic properties.** **a** Q-PCR data showing expression of EMT markers in 22RV1-*DLX1*-KO and control SCR cells. **b** Immunoblots showing vimentin and E-cadherin using same cells as **a**.  $\beta$ -actin was used as loading control. **c** Same as **b** except for cleaved PARP, cleaved Caspase-3 and Bcl-xL. **d** Flow cytometry-based apoptosis assay using 22RV1-*DLX1*-KO and control cells (top panel) and *DLX1*-silenced VCaP cells (bottom panel). **e** Flow cytometry data for cell cycle distribution using same cells as in **d**. **f** Q-PCR data for stem cell markers using same cells as **d**. **g** Flow cytometry data depicting ABCG2 (top panel) and CD44 (bottom panel) expression in *DLX1* overexpressing RWPE1 cells, 22RV1-*DLX1*-KO, and *DLX1* silenced VCaP cells. **h** Fluorescence intensity of catalyzed ALDH substrate in 22RV1-*DLX1*-KO and control cells. Marked windows show ALDH1+ percent cell population. **i** Same as **h**, except for *DLX1* silenced VCaP cells. **j** Q-PCR data showing expression of target genes in 22RV1-*DLX1*-KO and control cells ( $P < 0.0001$ ). **k** Schema showing chromosomal location of *DLX1* binding motif (DBM1/2) at the *ALDH1A1* (top) and *HNF1A* (bottom) promoters. **l** ChIP-qPCR data of *DLX1* (top panel) and H3K9Ac (bottom panel) on *ALDH1A1* in 22RV1-*DLX1*-KO and SCR control cells ( $P < 0.0001$ ). **m** Same as in **l** except for the *HNF1A* promoter.



Next, we examined the cell surface expression of two well-known stem cell markers, ABCG2 and CD44 in 22RV1-DLX1-KO, DLX1-silenced VCaP, and RWPE1-DLX1 cells. Interestingly, a marked reduction in the expression of ABCG2 (~30-60%) and CD44 (~50-80%) was observed in 22RV1-DLX1-KO and DLX1-silenced VCaP cells, while a robust increase in these markers was noted in RWPE1-DLX1 cells (Fig. 2g). Since increased aldehyde dehydrogenase 1A1 (ALDH1A1) activity is often associated with cancer stem cell phenotype<sup>6</sup>, we performed ALDH activity assay using 22RV1-DLX1-KO and DLX1-silenced VCaP cells showed reduction in the ALDH activity (Fig. 2h-i), indicating a plausible function of DLX1 in promoting cancer stemness. We also established the occupancy of DLX1 on the promoters of *ALDH1A1* and *HNF1A*, while reduced DLX1 enrichment and H3K9Ac, a transcriptional activation mark was noted in 22RV1-DLX1-KO cells (Fig. 2k-m). Hence, we establish *ALDH1A1* and *HNF1A* as the direct transcriptional targets of DLX1, which are also known to play critical role in stemness, embryonic development, and carcinogenesis<sup>7,8</sup>.

**Figure 3**

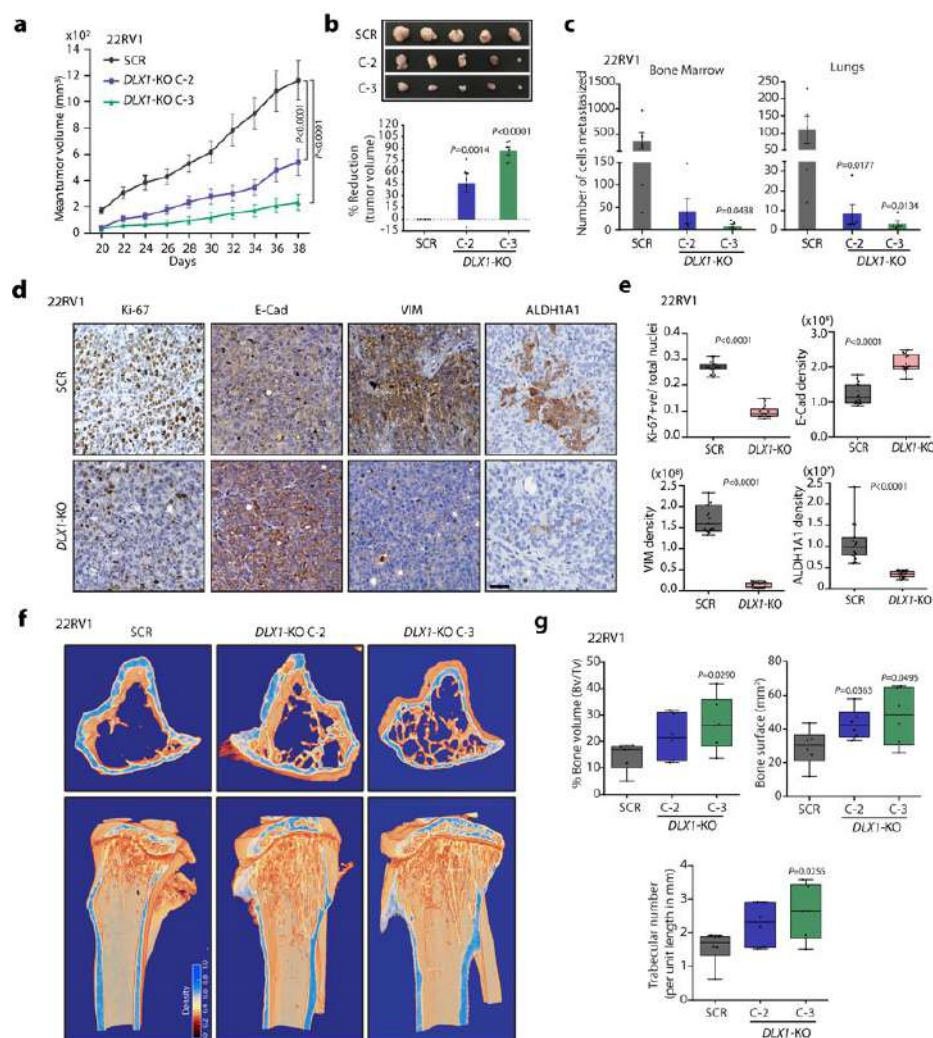


**Figure 3. Abrogating DLX1 expression results in tumor regression and reduced metastases. a** Mean tumor volume of 22RV1-DLX1-KO and control SCR cells subcutaneously implanted in NOD/SCID mice (n=6,  $P < 0.0001$ ). **b** Representative images of the tumors excised at end of the xenograft experiment (top panel). Bar graph showing relative percent reduction in tumor burden. **c** Bar graphs representing number of cells metastasized to the bone marrow and lungs in xenografted mice as labelled (n=5). **d** Images depicting immunostaining for Ki-67, E-cadherin (E-Cad), Vimentin (VIM), and ALDH1A1 on xenograft tumor sections, images are representative of 3 tissue samples. Scale bar, 35  $\mu$ m. **e** Box plots showing immunostaining quantification of Ki-67, E-Cad, VIM and ALDH1A1. Quantification was blindly done from 15 random histological fields ( $P < 0.0001$ ). **f** Representative microCT bone images showing horizontal section (top panel) and vertical cross-section (bottom panel) views of the tibia excised from mice (n=6) four weeks after intra-medullary tibia injection using 22RV1-DLX1-KO and control cells. **g** Same as f, except box plots showing bone architecture parameters analyzed using CTAn software.

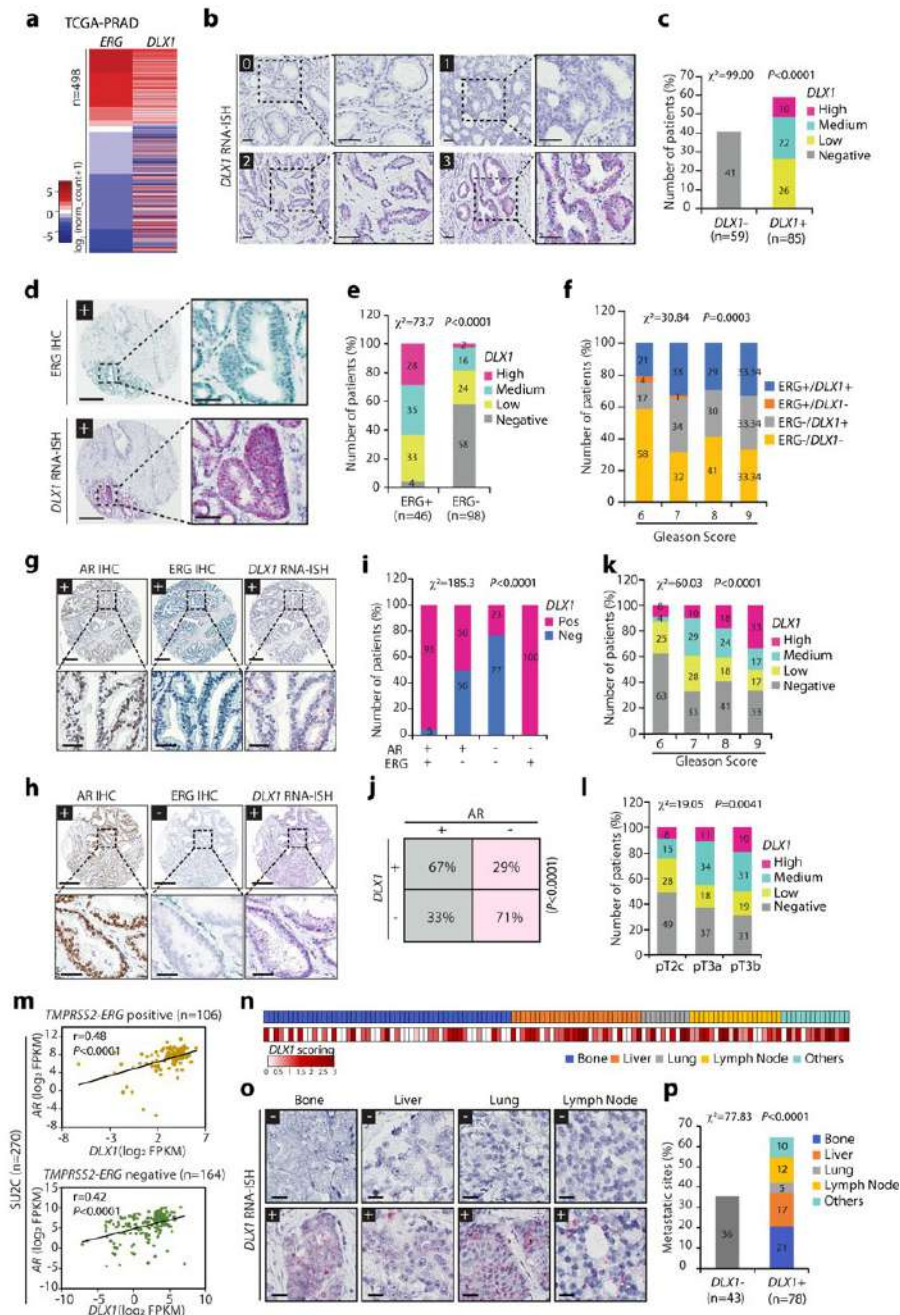
***DLX1 plays pivotal role in tumor growth and metastasis***

To examine the role of DLX1 in tumorigenesis, we performed mice xenograft experiment by implanting 22RV1-DLX1-KO or 22RV1-SCR control cells subcutaneously in the flank region of immunodeficient NOD/SCID mice and monitored the animals for tumor growth. A significant decrease in tumor growth with a notable ~80% reduction in tumor burden at the end of the study was observed in the 22RV1-DLX1-KO cells implanted group compared to the control group (Fig. 3a-b). A significant reduction in the number of cells metastasized to the bone marrow and lungs was observed in the 22RV1-DLX1-KO cells implanted group by human Alu-specific PCR (Fig. 3c). A significant reduction in Ki-67 expression, accompanied by reduced Vimentin and increased E-cadherin expression was observed in the tumors of the DLX1-KO group compared to control. Moreover, a significant decrease in the expression of DLX1 target, ALDH1A1 was also recorded in DLX1-KO tumor tissues (Fig. 3d-e).

Moreover, DLX1 has been reported to play a key role in osteoclastogenesis and bone-resorption<sup>9</sup>, which contributes to osteolytic effects in bone tumors and metastasis<sup>10</sup>. Hence, we next sought to determine the role of DLX1 using an experimental bone metastasis model, wherein intramedullary tibial injection was performed using 22RV1-SCR control and DLX1-KO cells in athymic NU-Foxn1<sup>nu</sup> nude mice. Four weeks post-injection, X-ray scans were taken and subsequently, excised tibia implanted with tumor cells were subjected to micro computed tomography (microCT), which showed higher bone loss in the control 22RV1-SCR group compared to DLX1-KO (Fig. 3f). Further, we examined the bone morphometric parameters of the metaphysis region of the tibia from both groups using CTAn (CT-Analyser) software. Interestingly, tibia implanted with DLX1-KO cells showed an increase in bone volume fraction (Bv/Tv), bone surface (BS), and trabecular number (TN) compared to tibia in the control group, thus signifying the presence of bone loss and destruction of bone architecture in 22RV1-SCR control group (Fig. 3g). Taken together, these findings provide a comprehensive understanding of DLX1 mediated oncogenicity and its possible role in PCa associated bone metastases.

***Elevated ERG and AR levels show positive association with DLX1 expression***

Stratification of the clinical genomic data of PCa patients (n=498) based on the expression of ERG revealed that most of the cases with higher ERG levels also exhibit increased expression of DLX1 transcript (Fig. 4a). Next, we performed IHC, and RNA in-situ hybridization (RNA-ISH) for ERG and DLX1 expression, respectively using a tissue microarray (TMA) comprising 144 PCa patient specimens, and all but three of these patients were hormone naïve. The RNA-ISH staining patterns for DLX1 were classified into four levels ranging from the score of 0 to 3, nearly ~60% of the patients were found positive for DLX1 expression ranging from low to high (Fig. 4b-c). About ~96% of the TMPRSS2-ERG fusion-positive cases showed positive staining for DLX1 expression (Fig. 4d-e), wherein ~28% patients showed high score for DLX1 (DLX1<sup>Hi</sup>, score 3), ~35% patients with moderate (DLX1<sup>Me</sup>, score 2) and ~33% patients with lower DLX1 expression (DLX1<sup>Lo</sup>, score 1) (Fig. 4e), suggesting a possible role of ERG in DLX1 regulation. In terms of clinical staging, the percentage of tumors stained positive for both ERG and DLX1 substantially increase from 21% in low Gleason score (GS6) to 33% in high Gleason score disease (GS9), similarly tumors stained positive only for DLX1 expression (ERG-/DLX1+) also exhibit higher Gleason score (Fig. 4f). Thus, suggesting that the majority of the PCa patients harboring higher DLX1 with/without ERG expression (ERG+/DLX1+ and ERG-/DLX1+) are associated with advanced stage disease.

**Figure 4**

**Figure 4. Elevated ERG and AR correlates with higher DLX1 levels representing advanced stage aggressive disease.** **a** Heatmap showing TCGA-PRAD RNA-Seq data for *ERG* and *DLX1* expression in primary PCa specimens (n=498). Shades of red and blue represent the log<sub>2</sub>(norm\_count+1) value. **b** Representative core of PCa tissue microarray (TMA) showing RNA in-situ hybridization (RNA-ISH) scoring pattern for *DLX1* in 144 PCa patient specimens, score 0 represents *DLX1* negative, score 1 signifies low *DLX1*, score 2 and score 3 represents medium and high *DLX1* expression, respectively. Scale bar, 50µm. **c** Bar plot showing percentage of patients negative (*DLX1*−) and positive (*DLX1*+) for *DLX1* expression based on the scoring pattern ( $P < 0.0001$ ). **d** Same as **b** except Immunohistochemistry (IHC) for ERG (top panel) and RNA-ISH for *DLX1* (bottom) in 144 PCa patient tissue specimens. **e** Bar plot showing percentage of patients with varying *DLX1* expression in ERG-positive (ERG+) and -negative (ERG−) PCa cases ( $P < 0.0001$ ). **f** Same as **e** except an association between ERG and *DLX1* expression status and Gleason scores of PCa patients ( $P = 0.0003$ ). **g** Same as **b** except representative tumor cores showing IHC for AR, ERG and RNA-ISH for *DLX1* representing AR+/ERG+/DLX1+ status in 144 PCa patient tissue specimens. **h** Same as **g** except for representative AR+/ERG−/DLX1+ patient in TMA containing 144 PCa specimens. **i** Bar plot depicting percentage of patients with positive and negative *DLX1* expression in AR+/− and ERG+/− respective background. Patients showing low, medium and high *DLX1* expression categorized as *DLX1*-positive ( $P < 0.0001$ ). **j** Contingency table for the AR and *DLX1* status in TMA patient specimens.  $P$ -value denotes Fisher's exact test ( $P < 0.0001$ ). **k** Bar plot showing association between *DLX1* expression and Gleason scores of tumor specimens ( $P < 0.0001$ ). **l** Same as **k**, except association of *DLX1* expression with tumor stage ( $P = 0.0041$ ). **m** Correlation plot of AR and *DLX1* using Stand Up To Cancer (SU2C) dataset by categorizing patients as *TMPS2-ERG* positive (top panel) and negative samples (bottom panel). **n** Heatmap showing *DLX1* levels in tumor specimens representing distant metastatic sites of metastatic CRPC patients. **o** Same as **n** except for RNA-ISH for *DLX1* expression in TMA containing 121 mCRPC biospecimens collected.

from various metastatic sites. Scale bar, 25µm. **p** Bar plot showing DLX1 expression in percent metastatic sites from CRPC patients same as **n** ( $P<0.0001$ ).

Next, the specimens categorized as AR+ were further examined for the presence or absence of ERG expression and/or *DLX1* expression by RNA-ISH (Fig. 4g-h). Interestingly, we found that ~95% of the patients (42 out of 44) positive for AR and ERG (AR+/ERG+) showed *DLX1* expression, similarly ~50% of the AR+/ERG- patients (36 out of 72) were also positive for *DLX1* (Fig. 4i), while this percentage decreased (~23%) for the patients (6 out of 26) whose tumors were negative for both AR and ERG (Fig. 4i-j). Moreover, *DLX1* level alone gradually increased as a function of disease stage; ~37% positive in GS6 disease to ~67% positive in GS9 disease (Fig. 4k), similarly, ~51% in pT2c (pathologic tumor 2c) to 69% in pT3b stage (Fig. 4l).

Providing the association of DLX1 with advanced stage disease, we analyzed Stand Up to Cancer (SU2C) metastatic PCa dataset publicly available on cBioPortal for the expression of *DLX1* and its correlation with *AR* and *ERG*<sup>11</sup>. A significant positive correlation between AR and *DLX1* expression was observed in metastatic PCa patients irrespective of *TMPRSS2-ERG* fusion status (Fig. 4m). Further, we performed RNA-ISH for *DLX1* in a metastatic PCa TMA comprising 121 metastatic sites collected from 45 patients (Fig. 4n-o). We found that ~64% of total metastatic sites showed *DLX1* expression, of these 21% belonged to bone, 17% to liver, 5% to lung, 12% to lymph node and 10% to other organ sites (Fig. 4p). Together, our data suggest a role of DLX1 in aggressive and metastatic PCa and indicate a plausible oncogenic cooperativity between DLX1, ERG, and AR in progression of this disease.

### ***ERG regulates DLX1 in TMPRSS2-ERG fusion-positive prostate cancer***

We next investigated the role of ERG in transcriptional regulation of *DLX1*, and analyzed publicly available ERG ChIP-Seq dataset in VCaP (*TMPRSS2-ERG* fusion-positive) cells<sup>12,13</sup>, and an increased enrichment of ERG on the *DLX1* promoter was observed (Fig. 5a). Furthermore, enrichment of ERG on the *DLX1* promoter was also observed in ectopic ERG overexpressing RWPE1 cells<sup>14</sup> (Fig. 5a). Next, our ChIP-qPCR data confirmed the significant recruitment of ERG at putative binding sites namely, EBM1 (P1) and EBM2 (P2) on the *DLX1* promoter in VCaP cells (Fig. 5b). To confirm whether ERG occupancy is associated with transcriptionally active chromatin, we examined the presence of transcriptional activation marks, and a marked enrichment of H3K9Ac along with RNA polymerase II (RNA-Pol II) was observed (Fig. 5b). In agreement with this, ectopic ERG overexpression in RWPE1 cells (RWPE1-ERG) resulted in upregulation of DLX1 both at the transcript and protein levels (Fig. 5c). As speculated, a significant increase in the reporter activity was observed in RWPE1-ERG cells transfected with a wild-type *DLX1* promoter reporter, while no significant change in the luciferase activity with mutated EBMs was observed (Fig. 5d).

Since AR signaling is known to drive the expression of ERG in *TMPRSS2-ERG* fusion-positive background, we next examined the effect of synthetic androgen methyltrienolone (R1881) on the expression of *DLX1* in VCaP cells. Notably, ~2-fold increase in DLX1 expression both at the transcript and protein levels was observed in R1881 stimulated VCaP cells (Fig. 5e-f). Next, we tested whether AR also plays a direct role in the transcriptional regulation of *DLX1* (Fig. 5g). Thus, to ascertain this, we analyzed ChIP-Seq datasets (GSE28951)<sup>15</sup> for AR and ERG in R1881 stimulated VCaP cells. Notably, a strong binding of AR on the third exon (chr2:172,661,000-172,662,500) of *DLX1* was observed in R1881 stimulated VCaP cells (Fig. 5h). We further examined the binding of AR on the *DLX1* gene using publicly available dataset (GSE70079)<sup>16</sup> comprising normal and PCa specimens, and a remarkable enrichment of AR was observed on the putative enhancer element of the



*DLX1* in PCa specimens (Fig. 5i). Conclusively, we show that ERG directly gets recruited on the *DLX1* promoter thereby regulating its expression in *TMPRSS2-ERG* positive cases. Our findings also imply the potential role of AR signaling in mediating *DLX1* expression in PCa.

**Figure 5**

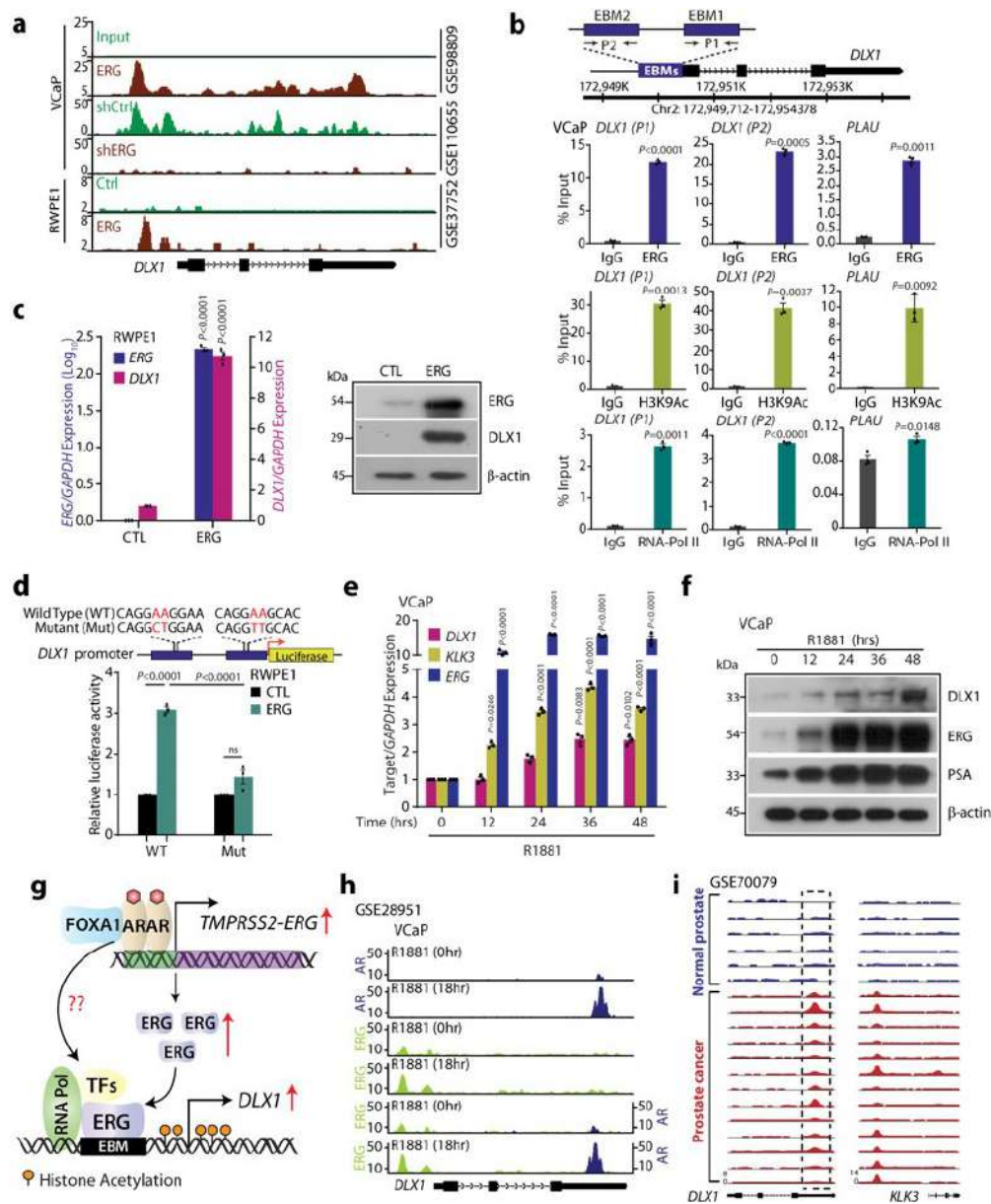


**Figure 5. *DLX1* is a transcriptional target of ERG in *TMPRSS2-ERG* positive prostate cancer.** **a** Chromatin immunoprecipitation-sequencing (ChIP-Seq) data depicting ERG enrichment at the *DLX1* promoter in the indicated cell lines from GEO databases (GSE98809, GSE110655 and GSE37752). **b** Schema showing chromosomal location of the ERG binding motifs (EBM) onto *DLX1* promoter selected for ChIP-qPCR (top panel). ChIP-qPCR data showing recruitment of ERG, histone H3 lysine 9 acetylation (H3K9Ac) and RNA-polymerase II (RNA-Pol II) at the *DLX1* and *PLAU* promoters. **c** Q-PCR (left panel) and immunoblot (right panel) data showing the expression of ERG and *DLX1* in RWPE1 cells overexpressing ERG ( $P < 0.0001$ ). **d** Schema showing site-directed mutagenesis of *DLX1* promoter cloned upstream of luciferase gene, nucleotides in red were mutated (top). Luciferase reporter assay indicating wild-type (WT) and mutant (Mut) *DLX1* promoter-driven reporter activity (bottom panel) in ERG overexpressing and control RWPE1 cells ( $P < 0.0001$ ). **e** Q-PCR data showing relative expression of target genes in VCaP cells stimulated with 10nM R1881 at the indicated time points. **f** Same as e, except immunoblot data. **g** Schematic diagram depicting ERG-mediated transcriptional regulation of *DLX1* and plausible role of AR in *DLX1* regulation. **h** ChIP-Seq data (GSE28951) showing recruitment of AR and ERG on the *DLX1* promoter in R1881 stimulated VCaP cells. **i** ChIP-Seq data (GSE70079) showing enrichment of AR at the *DLX1* putative enhancer in the normal prostate (n=6) and PCa (n=13) tissue specimens. *KLK3* represents positive control.



**Androgen receptor regulates *DLX1* expression in prostate cancer.** Considering an association between AR and *DLX1* expression in PCa specimens and AR occupancy at the *DLX1* enhancer region, we next sought to examine the role of androgen signaling in the regulation of *DLX1*. To further validate the AR binding on the putative enhancer of *DLX1*, we performed ChIP-qPCR using R1881-stimulated VCaP cells, identifying a significant enrichment of AR on the *DLX1* enhancer, which was disrupted upon anti-androgen enzalutamide (Enza) treatment (Fig. 6a). As speculated, treatment of VCaP cells with Enza and EPI-001 abrogated R1881-induced *DLX1* expression, implicating the role of AR in transcriptional regulation of *DLX1* (Fig. 6b).

Figure 6

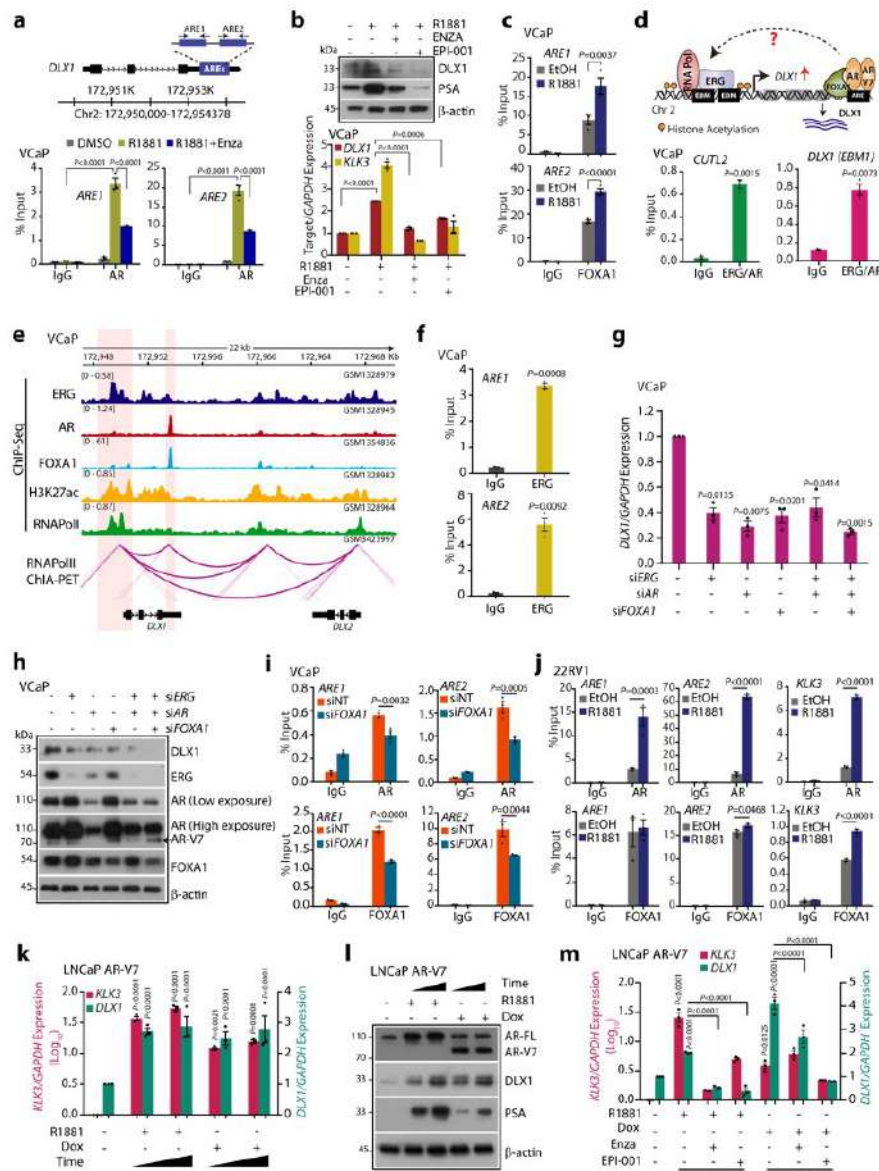


**Figure 6. AR and AR-V7 regulate *DLX1* expression in both ERG-dependent and -independent manner.** **a** Schematic showing the androgen response elements (AREs) at the *DLX1* putative enhancer (top panel). ChIP-qPCR data (bottom panel) depicting AR recruitment at the *DLX1* putative enhancer in R1881 (10nM) stimulated VCaP cells in the presence or absence of Enzalutamide (Enza, 10μM) ( $P < 0.0001$ ). **b** Immunoblot (top panel) and Q-PCR (bottom panel) data showing relative expression of target genes in VCaP cells under similar culture conditions as indicated. **c** ChIP-qPCR data depicting FOXA1 recruitment at the *DLX1* putative enhancer in R1881 (10nM) stimulated VCaP. **d** Schematic representation showing the possible interaction between ERG and AR on the *DLX1* promoter (top panel). Re-ChIP data showing co-enrichment of AR and ERG on EBM at the *DLX1* promoter (bottom panel). **e** Integrated genome view of 3D chromatin structure and binding of transcription factors at the genomic and nearby region of *DLX1*. **f** Bar plots depicting ChIP-qPCR data for ERG occupancy at the *DLX1* enhancer region. **g** Q-PCR data showing relative expression of *DLX1* in siRNA-mediated *ERG*, *AR* and/or *FOXA1* silenced VCaP cells. **h** Same as **g** except immunoblot data. **i** ChIP-qPCR data showing enrichment of AR (top panel) and FOXA1 (bottom panel) in siRNA-mediated *FOXA1* silenced VCaP cells. **j**

ChIP-qPCR data depicting AR (top panel) and FOXA1 (bottom panel) enrichment at the *DLX1* putative enhancer in 22RV1 cells stimulated with R1881 (10nM) for 16 hours. *KLK3* shown as a positive control. **k** Relative expression of *KLK3* and *DLX1* in doxycycline (Dox) induced AR-V7 overexpressing LNCaP cells treated with R1881 (10nM). For induction, 40ng/ml of Dox or vehicle control was used for 24 and 48 hours. **l** Immunoblots showing the expression of AR-FL, AR-V7, DLX1 and PSA using same cells as **k**.  $\beta$ -actin used as loading control. **m** Q-PCR data showing *DLX1* and *KLK3* expression in LNCaP AR-V7 cells under similar culture conditions as mentioned at 48-hour time point.

Since FOXA1 is a known pioneer TF and a coactivator of AR<sup>17</sup>, we next investigated the occupancy of FOXA1 at the *DLX1* putative enhancer region. Importantly, ChIP-qPCR in VCaP cells show FOXA1 enrichment on the same locus, signifying the recruitment of AR transcriptional complex on the putative enhancer region of *DLX1* (Fig. 6c). Since AR and ERG interaction as a coregulatory TF is known to regulate the expression of common target genes<sup>18,19</sup>, we examined the probable co-interaction of ERG and AR at the *DLX1* promoter by performing re-ChIP experiment (Fig. 6d). As anticipated, ChIP using ERG antibody followed by pulldown using an AR antibody showed significant enrichment of AR and ERG at the *DLX1* promoter, thus confirming their interaction through the promoter-enhancer region (Fig. 6d). To further validate the plausible chromatin interaction at the *DLX1* genomic region, we analyzed the 3D-chromatin landscape of RNA-Pol II in VCaP cells using ChIA-PET dataset (GSE121020)<sup>20</sup>. Consistent with our findings, the RNA-Pol II ChIA-PET data confirmed the promoter-enhancer interaction at the *DLX1* gene, which also indicated the binding of ERG, AR, and FOXA1 transcription factors (Fig. 6e). Owing to the promoter-enhancer interaction at *DLX1* gene loci and ERG occupancy at *DLX1* enhancer region in ChIP-Seq data (Fig. 6e), we carried out ChIP-qPCR for ERG at the *DLX1* enhancer region. As expected, we observed notable enrichment of ERG at the enhancer region of *DLX1* (Fig. 6f). Remarkably, siRNA mediated knockdown of these regulatory factors namely, *ERG*, *AR* and *FOXA1* in VCaP cells in reduced DLX1 expression across all siRNA conditions (Fig. 6g-h). Also, pronounced decrease in the level of DLX1 was achieved by concurrent silencing of all the three key regulators (*ERG*, *AR*, and *FOXA1*), thereby indicating the transcriptional interplay between these factors. Collectively, our results suggest ERG and AR-mediated transcriptional co-regulation of *DLX1* in *TMPRSS2-ERG* fusion-positive cells. Moreover, upon androgen stimulation, enrichment of AR and FOXA1 was observed in *TMPRSS2-ERG* fusion-negative 22RV1 cells, suggesting the significance of AR signaling in transcriptional regulation of *DLX1* in an ERG-independent manner (Fig. 6j).

Furthermore, using an inducible expression system for AR-V7, we generated LNCaP cells that can express both AR-FL and AR-V7, which mimics the clinical state of the majority of PCa patients with resistance to enzalutamide or abiraterone<sup>21</sup>. In these genetically engineered LNCaP cells, the expression levels of AR-FL and AR-V7 can be induced by treating them with R1881 and doxycycline (dox), respectively (Fig. 6k). In line with this, both AR-FL, as well as AR-V7 expression, led to increased expression of DLX1 transcript and protein levels (Fig. 6k-l). As we conjecture, treating LNCaP AR-V7 cells with AR antagonists (enzalutamide or EPI-001) in the presence of R1881 or dox abrogated AR-FL and AR-V7 mediated increase in DLX1 expression (Fig. 6m). Taken together, our findings suggest a role of AR-FL and AR-V7 in the transcriptional regulation of *DLX1* in ERG-dependent as well as -independent manner. These findings also highlight the critical role of AR-V7 in the transcriptional regulation of *DLX1*, thereby resonating with relatively high DLX1 expression in PCa patients with advanced stage disease and higher Gleason score.

### ***BETi attenuates DLX1 expression and its oncogenic properties***

Since the utility of BETi, namely JQ1 and I-BET762 has been shown to inhibit aberrant AR signaling and the localization of BRD4 to AR target genes<sup>22</sup>, we sought to investigate the ability of JQ1 in impeding the transcriptional regulators of *DLX1*, namely ERG and AR. Using ChIP-Seq

dataset (GSE55064)<sup>22</sup>, we examined the recruitment of ERG on *DLX1* promoter following BETi treatment in VCaP cells. Interestingly, a remarkable decrease in the enrichment of ERG was observed in JQ1 treated VCaP cells compared to control (Fig. 7a).

**Figure 7**

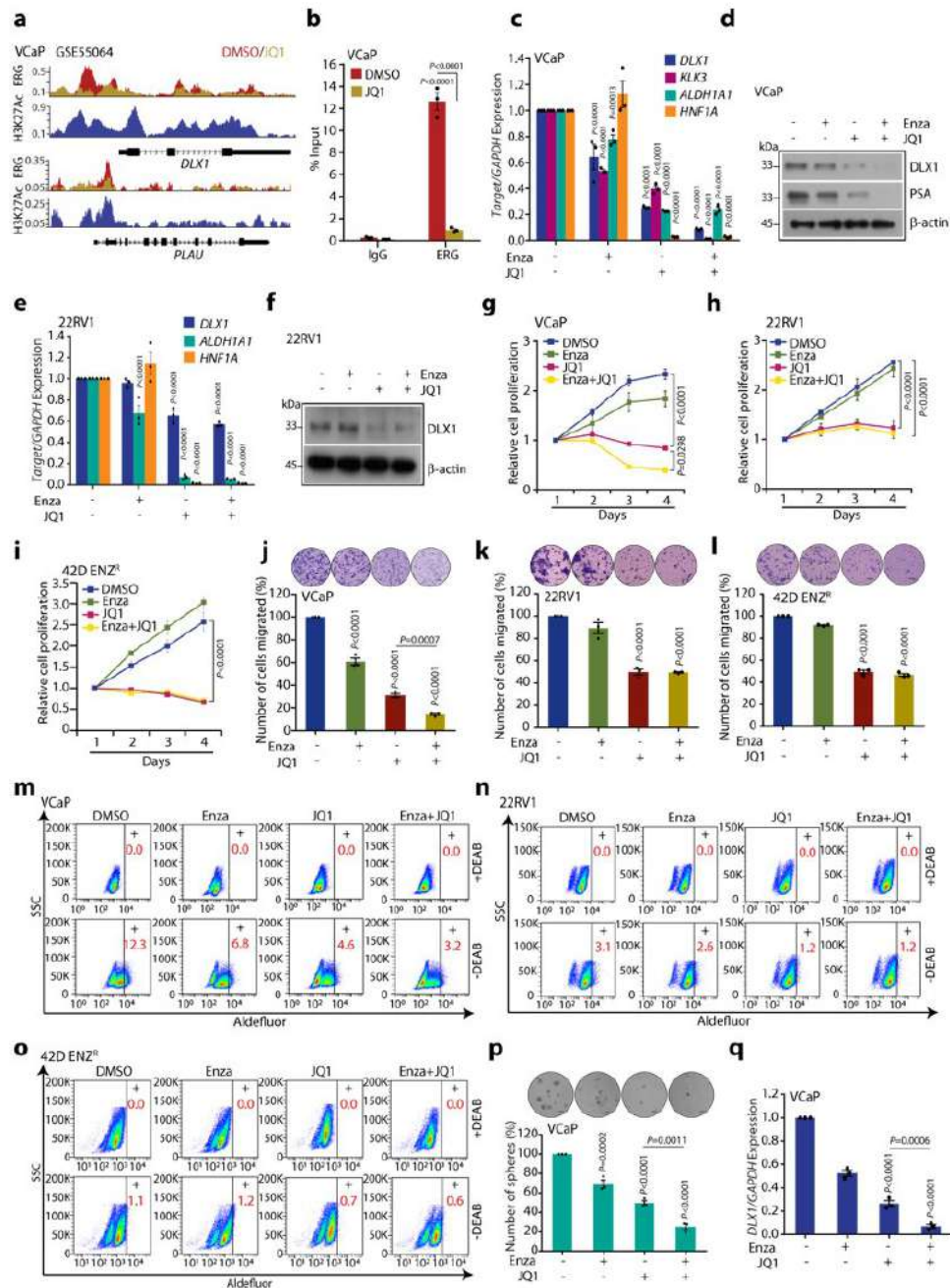


**Figure 7. BET inhibitor alone or in combination with Enzalutamide downregulates *DLX1* expression and mitigates its oncogenic properties.** **a** ChIP-Seq data (GSE55064) showing ERG enrichment on *DLX1* promoter in VCaP cells treated with JQ1 or vehicle control for 24 hours. H3K27Ac represents active promoter in untreated cells. *PLAU* used as a positive control. **b** ChIP-qPCR data showing relative ERG enrichment on *DLX1* promoter in VCaP cells treated with JQ1 (0.5μM) for 48 hours ( $P < 0.0001$ ). **c** Q-PCR data showing relative expression of target genes in VCaP cells treated with Enza (10μM), JQ1 (0.5μM) alone or in combination for 48 hours. *KLK3* used as a positive control for JQ1 treatment. **d** Same as **c** except immunoblot. β-actin was used as loading control. **e** Same as **c** except 22RV1 cells. **f** Same as **e** except immunoblot ( $P < 0.0001$ ). **g** Cell proliferation assay in VCaP cells treated with drug conditions as mentioned in **c**. **h** Same as **g** except 22RV1 cells ( $P < 0.0001$ ). **i** Same as **g** except 42D ENZ<sup>R</sup> cells ( $P < 0.0001$ ). **j** Boyden Chamber Matrigel migration assay in VCaP cells using same treatment conditions as **c**. Inset shows representative image of the migrated cells (scale bar 30μm). **k** Same as **j** except 22RV1 cells (scale bar 30μm,  $P < 0.0001$ ). **l** Same as **j** except 42D ENZ<sup>R</sup> cells (scale bar 30μm,  $P < 0.0001$ ). **m** Fluorescence intensity of the catalyzed ALDH substrate in VCaP cells under same treatment conditions as **c**. Marked windows show ALDH1+ percent cell population. **n** Same as **m** except 22RV1 cells. **o** Same as **m** except 42D ENZ<sup>R</sup> cells. **p** Bar plot showing number of spheres formed in prostatosphere assay using VCaP under same treatment conditions as **c**. Inset shows representative image of the spheres formed (scale bar 100μm). **q** Q-PCR data for the *DLX1* expression using RNA isolated from VCaP prostatospheres.



Further, these results were confirmed by ChIP-qPCR for ERG using JQ1 treated VCaP cells, and a similar trend was observed (Fig. 7b). Recent preclinical and phase Ib/IIa clinical studies reported the efficacy of BET inhibitors in combination with anti-androgens in CRPC patients<sup>23,24</sup>. Hence, we examined whether JQ1 along with Enza could be effective in attenuating DLX1 expression and its oncogenic properties. Thus, we treated VCaP cells (*TMPRSS2-ERG* positive) with JQ1 alone or with Enza and examined the expression of DLX1 and its target genes. Intriguingly, we observed ~60% reduction in *DLX1* expression as well as a concomitant decrease in the expression of DLX1 target genes, namely *ALDH1A1* and *HNF1A* in JQ1 treated VCaP cells compared to vehicle control (Fig. 7c). Although this effect was more pronounced (~90%) when VCaP cells were treated with JQ1 and Enza combination (Fig. 7c-d).

**Figure 8**

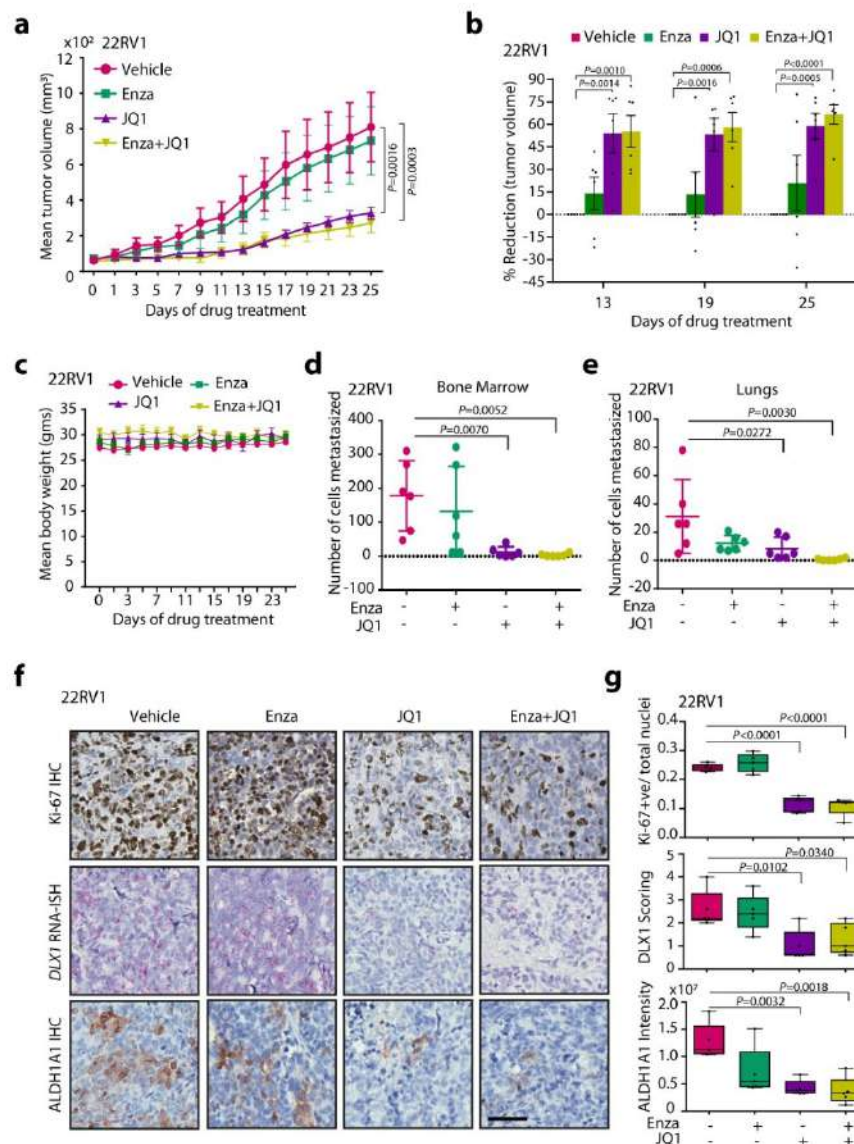


**Figure 8. BET inhibitor alone or in combination with Enzalutamide attenuates DLX1-mediated tumorigenesis and metastases.** **a** Mean tumor volume of xenografts generated by implanting 22RV1 cells in athymic nude mice, and randomized into four treatment groups (n=6 each), namely, vehicle control, Enza (20mg/kg), JQ1 (50mg/kg), and a combination of Enza and JQ1. **b** Bar plot showing percent tumor reduction in the treatment groups (n=6) compared with vehicle control group. **c** Mean body weight of mice (n=6 per group) during treated with drugs as mentioned in **a**. **d** Scatter dot plot showing number of cells metastasized to bone in xenografted mice treated with drugs (n=6 per group) as mentioned in **a**. Data represents mean ± SD. **e** Same as **d** except cells metastasized to lungs (n=6 per group). **f** Representative images depicting IHC staining for Ki-67, ALDH1A1, and RNA-ISH for *DLX1* using formalin-fixed paraffin-embedded tumor xenograft specimens (n=5 per group) as **a**. Scale bar, 50µm. **g** Box plots showing quantification of Ki-67, ALDH1A1 and *DLX1* expression in the tumor tissue sections (n=5) of the mice xenografts as **a**.

Further, to investigate the JQ1 inhibitory effect in ERG-independent background, we treated castrate-resistant 22RV1 cells (ERG-negative) with both BETi and Enza. As speculated, a similar inhibitory effect in the expression of *DLX1*, *ALDH1A1*, and *HNF1A* was observed with JQ1 and/or Enza, indicating the absence of combinatorial additive effects as in case of VCaP cells (Fig. 7e-f). Likewise, treatment of VCaP, 22RV1, and 42D ENZ<sup>R</sup> cells with JQ1 and/or Enza showed a decrease in the cell migratory and foci forming abilities, although this inhibitory effect was more evident in VCaP cells treated with the drug combination (Fig. 7j-l). Interestingly, reduced levels of ALDH activity were noted in these cells treated with JQ1 alone, while drug combination showed slightly enhanced effect only in the ERG-positive VCaP cells (Fig. 7m-o). Since ALDHs play a critical role in the maintenance and differentiation of stem cells, we evaluated the efficacy of these two drugs in *in vitro* using a 3D-prostatosphere assay using VCaP cells. Notably, a significantly decreased number of spheres were formed in cells treated with drug combination than JQ1 alone (Fig. 7p). Moreover, reduced tumor-sphere forming ability of VCaP cells treated with drug combination group was corroborated by robust decrease in *DLX1* expression compared to JQ1 alone (Fig. 7q). Collectively, our data reveal the efficacy of JQ1 alone or in combination with Enza for targeting DLX1-driven PCa in an ERG-dependent and -independent manner.

**Figure 9**

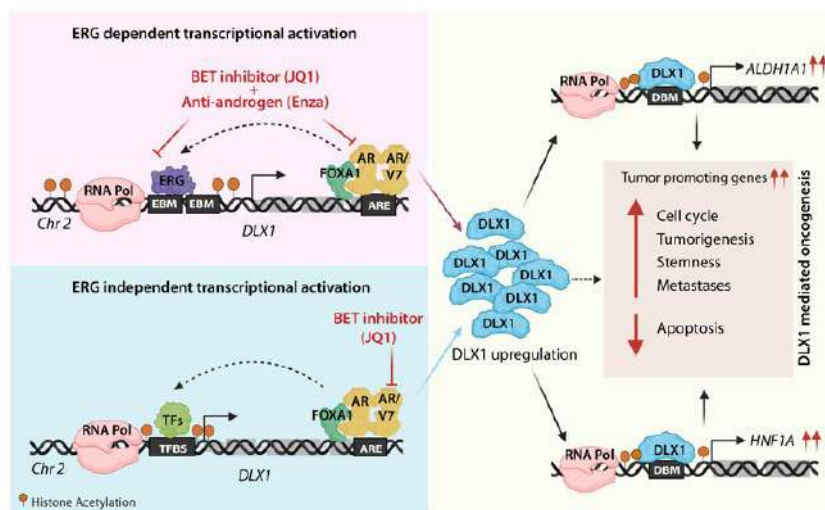


**Figure 9. Schematic showing transcriptional regulation of *DLX1* and therapeutic utility of BET inhibitor and anti-androgen in suppressing *DLX1*-mediated oncogenic effects.** Illustration depicting transcriptional regulation of *DLX1* via ERG and AR driven circuitry in ERG fusion-positive background, and through AR/FOXA1 in an ERG-independent context, thereby promoting cancer progression and metastases. Additionally, *DLX1* drives the expression of its target genes involved in stemness and oncogenesis, such as *ALDH1A1* and *HNF1A*. Utility of BET inhibitor alone or in combination with anti-androgen drugs to target transcriptional regulators of *DLX1* resulting in reduced expression of *DLX1* and its downstream oncogenesis.

### ***BETi abrogates *DLX1*-mediated tumorigenesis and metastases in mice***

To investigate the efficacy of BETi against *DLX1*-mediated tumor growth *in vivo*, we implanted 22RV1 cells subcutaneously in athymic immunodeficient mice, and when the tumors reached a palpable stage (average volume ~75 mm<sup>3</sup>); mice were randomized into four groups (n=6) and the drugs were administered. We observed that the mice treated with JQ1 alone or a combination of JQ1 and Enza showed almost similar trend in tumor regression (~50% and ~60% at day 19 and 25, respectively) as compared to the vehicle control group, indicating absence of any additive effect with the combinatorial treatment (Fig. 8a-b). Next, to determine the impact of drug treatment on spontaneous tumor metastasis, we excised lungs and bone marrow from the mice after terminating the study and isolated genomic DNA, followed by quantitative PCR for detecting human specific

*Alu*-sequence. We observed a marked decrease in the number of cells metastasized to these organs in both JQ1 alone, or in combination with Enza groups compared to vehicle control (Fig. 8d-e). Notably, no enhanced effect was observed in the group treated with drug combination. Subsequently, to investigate the effect of these drugs in the tumor xenografts, we performed IHC staining for cell proliferative marker Ki-67, ALDH1A1, and RNA-ISH for *DLX1* expression. As speculated, a significant decrease in the *DLX1* expression, accompanied by reduced Ki-67 and ALDH1A1 expression was noted in JQ1 alone as well as in drug combination groups (Fig. 8f-g). Thus, our *in vivo* findings establish the therapeutic utility of BETi and anti-androgen in hampering the DLX1-mediated tumorigenesis and metastases.

### Impact of the research in the advancement of knowledge or benefit to mankind

We unraveled ERG- and AR-mediated regulatory mechanisms involved in upregulation of DLX1 in an aggressive subset of PCa patients. We demonstrate that AR along with FOXA1 interacts with ERG as a coregulatory transcription factor, thereby orchestrating *DLX1* expression in *TMPRSS2-ERG* positive background. While, in fusion-negative background, AR and FOXA1 function in an ERG-independent manner, possibly in association with other coregulatory factor(s) to regulate the expression of *DLX1*. Thus, this triad of the key regulators control DLX1 expression in a context-dependent manner, resulting in DLX1-mediated oncogenesis via upregulation of several DLX1 target genes and biological processes. Importantly, we also demonstrate pharmacological inhibition of DLX1 transcriptional circuitry by BET inhibitor in an ERG-independent background, and in combination with anti-androgen in an ERG-dependent context (Fig. 9).

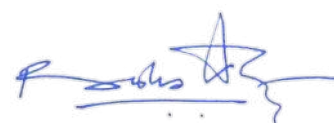
Currently, therapeutic targeting of bromodomain proteins has gained clinical importance for the treatment of several malignancies including CRPC, for instance, BETi such as OTX-015, ZEN003694, and GS-5829 are already in clinical trials as single agents or in combination with anti-androgens for CRPC patients<sup>25</sup>. Alongside, our results demonstrate the potency of BETi alone and in combination with anti-androgen to reduce the expression of DLX1 and its target genes, thus, implicating the utility of DLX1 as a therapeutic target. Concomitantly, we also suggest that the enhanced effectiveness of drug combination (BETi and anti-androgen) is plausibly predominant in *ERG* fusion-positive background. Our findings show that BETi along with anti-androgens could be used to mitigate the oncogenic effects of DLX1 via disrupting AR and ERG transcriptional circuitries and can be considered as a potential therapeutic intervention in the treatment of the ERG+/DLX1+ subtype of PCa. This study provided strong evidence to employ parallel treatment regimen with BETi or/and AR targeted therapeutics for the clinical management of DLX1-positive PCa subtype, hence opening new treatment avenues for patients with advanced stage disease.

### References

- 1 Panganiban, G. & Rubenstein, J. L. Developmental functions of the Distal-less/Dlx homeobox genes. *Development* **129**, 4371-4386 (2002).
- 2 Abate-Shen, C. Deregulated homeobox gene expression in cancer: cause or consequence? *Nature reviews. Cancer* **2**, 777-785, doi:10.1038/nrc907 (2002).
- 3 Chiba, S. *et al.* Homeoprotein DLX-1 interacts with Smad4 and blocks a signaling pathway from activin A in hematopoietic cells. *Proceedings of the National Academy of Sciences of the United States of America* **100**, 15577-15582, doi:10.1073/pnas.2536757100 (2003).
- 4 Liang, M. *et al.* DLX1, a binding protein of beta-catenin, promoted the growth and migration of prostate cancer cells. *Experimental cell research* **363**, 26-32 (2018).
- 5 Van Neste, L. *et al.* Detection of high-grade prostate cancer using a urinary molecular biomarker-based risk score. *European urology* **70**, 740-748 (2016).
- 6 Li, T. *et al.* ALDH1A1 is a marker for malignant prostate stem cells and predictor of prostate cancer patients' outcome. *Laboratory investigation* **90**, 234 (2010).



- 7 Tomita, H., Tanaka, K., Tanaka, T. & Hara, A. Aldehyde dehydrogenase 1A1 in stem cells and cancer. *Oncotarget* **7**, 11018 (2016).
- 8 Abel, E. V. *et al.* HNF1A is a novel oncogene that regulates human pancreatic cancer stem cell properties. *Elife* **7**, e33947 (2018).
- 9 Lézot, F. *et al.* Dlx homeobox gene family expression in osteoclasts. *Journal of cellular physiology* **223**, 779-787 (2010).
- 10 Wang, M., Xia, F., Wei, Y. & Wei, X. Molecular mechanisms and clinical management of cancer bone metastasis. *Bone Research* **8**, 1-20 (2020).
- 11 Abida, W. *et al.* Genomic correlates of clinical outcome in advanced prostate cancer. *Proceedings of the National Academy of Sciences* **116**, 11428-11436 (2019).
- 12 Bose, R. *et al.* ERF mutations reveal a balance of ETS factors controlling prostate oncogenesis. *Nature* **546**, 671-675 (2017).
- 13 Sandoval, G. J. *et al.* Binding of TMPRSS2-ERG to BAF chromatin remodeling complexes mediates prostate oncogenesis. *Molecular cell* **71**, 554-566. e557 (2018).
- 14 Rickman, D. S. *et al.* Oncogene-mediated alterations in chromatin conformation. *Proceedings of the National Academy of Sciences* **109**, 9083-9088 (2012).
- 15 Chng, K. R. *et al.* A transcriptional repressor co-regulatory network governing androgen response in prostate cancers. *The EMBO journal* **31**, 2810-2823 (2012).
- 16 Pomerantz, M. M. *et al.* The androgen receptor cistrome is extensively reprogrammed in human prostate tumorigenesis. *Nature genetics* **47**, 1346 (2015).
- 17 Jin, H.-J., Zhao, J. C., Wu, L., Kim, J. & Yu, J. Cooperativity and equilibrium with FOXA1 define the androgen receptor transcriptional program. *Nature communications* **5**, 3972 (2014).
- 18 Yu, J. *et al.* An integrated network of androgen receptor, polycomb, and TMPRSS2-ERG gene fusions in prostate cancer progression. *Cancer cell* **17**, 443-454 (2010).
- 19 Zhang, Z. *et al.* An AR-ERG transcriptional signature defined by long-range chromatin interactomes in prostate cancer cells. *Genome research* **29**, 223-235 (2019).
- 20 Ramanand, S. G. *et al.* The landscape of RNA polymerase II associated chromatin interactions in prostate cancer. *The Journal of Clinical Investigation* (2020).
- 21 He, Y. *et al.* Androgen receptor splice variants bind to constitutively open chromatin and promote abiraterone-resistant growth of prostate cancer. *Nucleic acids research* **46**, 1895-1911 (2018).
- 22 Asangani, I. A. *et al.* Therapeutic targeting of BET bromodomain proteins in castration-resistant prostate cancer. *Nature* **510**, 278 (2014).
- 23 Aggarwal, R. R. *et al.* A Phase Ib/IIa Study of the Pan-BET Inhibitor ZEN-3694 in Combination with Enzalutamide in Patients with Metastatic Castration-resistant Prostate Cancer. *Clinical Cancer Research* **26**, 5338-5347 (2020).
- 24 Asangani, I. A. *et al.* BET bromodomain inhibitors enhance efficacy and disrupt resistance to AR antagonists in the treatment of prostate cancer. *Molecular Cancer Research* **14**, 324-331 (2016).
- 25 Stathis, A. & Bertoni, F. BET proteins as targets for anticancer treatment. *Cancer discovery* **8**, 24-36 (2018).



**Publication #2:** Tiwari R<sup>†</sup>, Manzar N<sup>†</sup>, Bhatia V, Yadav A, Nengroo MA, Datta D, Carskadon S, Gupta N, Sigouros M, Khani F, Poutanen M, Zoubeidi A, Beltran H, Palanisamy N, Ateeq B\*. Androgen deprivation upregulates SPINK1 expression and potentiates cellular plasticity in prostate cancer. *Nature Communications*. 2020 Jan 20;11(1):384. <sup>†</sup>Co-first authors. **Impact Factor: 14.919.**

Overexpression of SPINK1 (Serine Peptidase Inhibitor, Kazal type 1) constitutes a substantial ~10-25% of the total PCa cases exclusively in *ETS*-fusion negative subtype<sup>26,27</sup>. Moreover, the expression of SPINK1 and ERG were shown in two distinct foci within a prostate gland, indicating that these two events are either independent or SPINK1 overexpression to be a sub-clonal event after *TMPRSS2-ERG* fusion<sup>28</sup>. Notably, SPINK1-positive patients show rapid progression to castration resistance and biochemical recurrence compared to *ETS*-fusion positive cases<sup>26,29,30</sup>. Androgen deprivation therapy (ADT) remains the gold-standard for treating advanced PCa, however the disease often progresses as castrate-resistant prostate cancer (CRPC), associated with poor prognosis<sup>31,32</sup>. Current treatment regimen for CRPC patients include enzalutamide (MDV3100) and apalutamide (ARN-509) (which blocks AR nuclear translocation and its genomic binding), and abiraterone acetate (an irreversible steroidal CYP17A1 inhibitor, that targets adrenal and intratumoral androgen biosynthesis)<sup>33-35</sup>. Although, these AR-targeted therapies are known to prolong the overall survival of patients, the response is temporary, and the disease eventually progresses. A subset of CRPC patients (~20% of advanced drug-resistant cases) escape the selective pressure of AR-targeted therapies by minimizing the dependency on AR signaling and often through lineage plasticity and acquisition of a neuroendocrine PCa (NEPC) phenotype. Treatment-related NEPC is associated with poor prognosis and patient outcome<sup>36</sup>. NEPC exhibits a distinct phenotype characterized by reduced or no expression of AR and AR-regulated genes, and increased expression of NEPC markers such as synaptophysin (SYP), chromogranin A (CHGA), and enolase 2 (ENO2)<sup>37</sup>.

Although, overexpression of SPINK1, which is seen in ~10-25% of PCa patients, has been associated with adverse clinical outcomes, the regulatory mechanism and the functional significance of SPINK1 upregulation remains largely unexplored. In this study, we discover that *SPINK1* is transcriptionally repressed by the AR and its co-repressor REST, and AR-antagonists relieve this repression leading to SPINK1 upregulation. Moreover, we identify that reprogramming factor SOX2 positively regulates *SPINK1* during NE-transdifferentiation. Notably, we also show elevated SPINK1 levels in androgen-signaling ablated mice xenograft models and NEPC patients, highlighting its possible role in cellular plasticity and development of the NEPC phenotype. Collectively, our findings draw attention towards the widespread use of AR antagonists and the plausible emergence of a distinct resistance mechanism associated with ADT-induced SPINK1 upregulation in prostate cancer.

### ***SPINK1 and AR are inversely correlated in PCa patients***

We discovered the possible link between *SPINK1* and *AR* expression in PCa patients, and stratified patients available at TCGA-PRAD (The Cancer Genome Atlas Prostate Adenocarcinoma) cohort based on high and low expression of *AR*. The patients with higher expression of *AR* showed a significantly lower expression of *SPINK1* and contrariwise (Fig. 1a). To further confirm this association, we performed immunohistochemical (IHC) analysis for the expression of SPINK1 and AR on tissue microarrays (TMA) comprising PCa patient specimens (n=237). Important to note that all of these cases underwent radical prostatectomy without any hormone or radiation therapy. In concordance with TCGA data analysis, our IHC findings reveal that SPINK1-positive patients exhibit low or negative staining for AR expression, while SPINK1-negative patients show high or medium

AR staining (Fig. 1b and Supplementary Fig. 1a). Importantly, about ~67% of the SPINK1+ patients (34 out of 51) demonstrate either low or negative staining for AR expression (Fig. 1c, d).

**Figure 1**

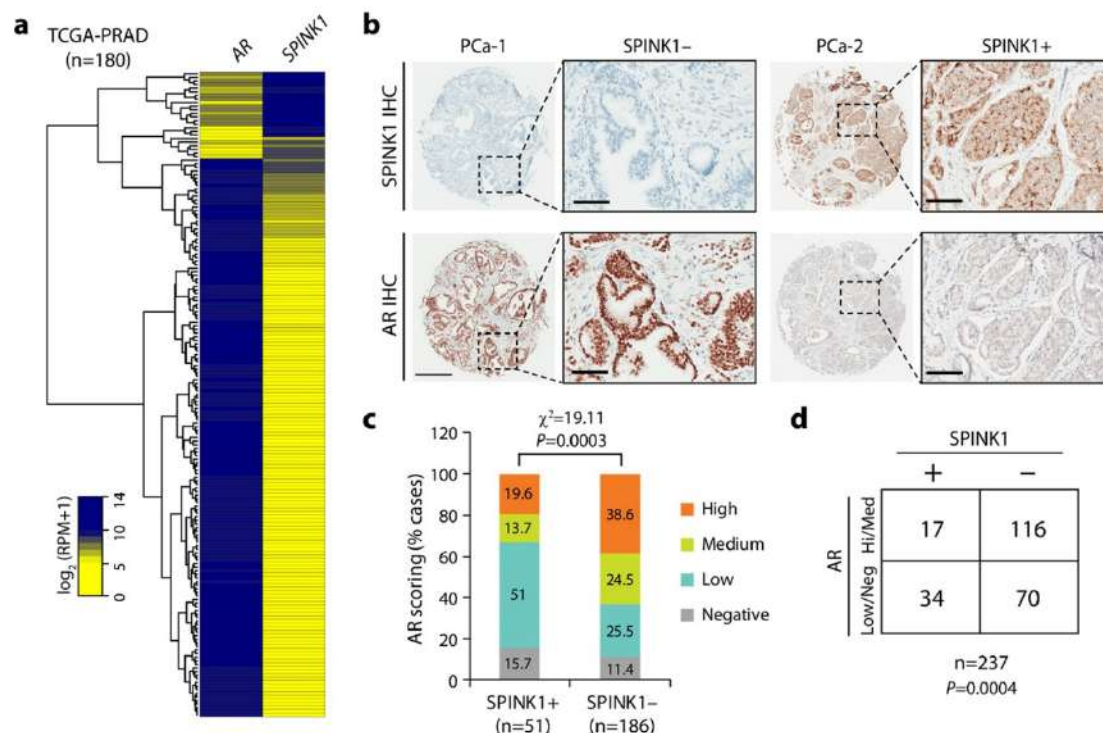


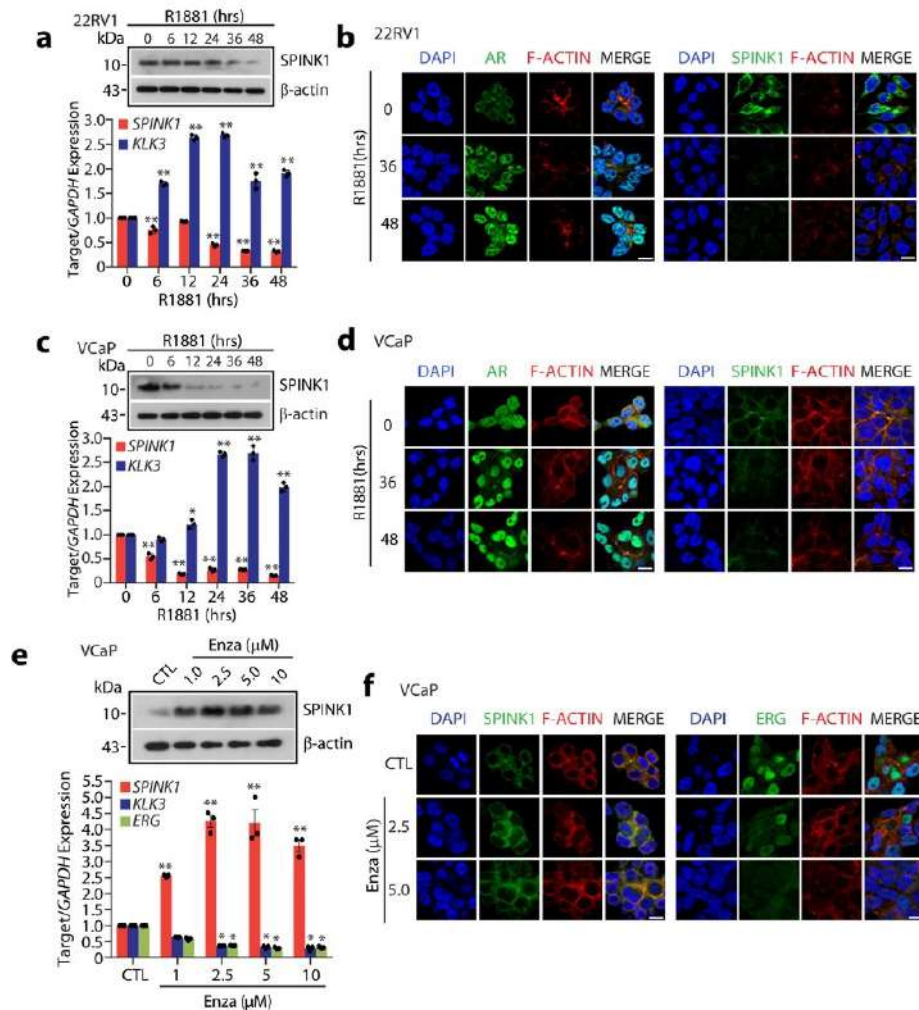
**Figure 1. SPINK1 is negatively correlated with AR in PCa patients.** (a) Heatmap depicting *AR* and *SPINK1* expression in TCGA-PRAD cohort (n=180). Shades of yellow and blue represents expression values in  $\log_2(\text{RPM}+1)$ . (b) Representative micrographs depicting PCa tissue microarray (TMA) cores (n=237), immunostained for SPINK1 and AR expression by immunohistochemistry (IHC). Top panel shows representative IHC for SPINK1 in SPINK1-negative (SPINK1-) and SPINK1-positive (SPINK1+) patients. Bottom panel represents IHC for AR expression in the tumor core from same patients. Scale bar represents 500μm and 100μm for the entire core and the inset images, respectively. (c) Bar plot showing percentage of IHC scoring for AR in the SPINK1+ and SPINK1- patients' specimens. *P*-value for the Chi-Square test is indicated. (d) Contingency table for the AR and SPINK1 status. Patients showing high or medium expression of AR were grouped as AR-(Hi/Med), while patients with low or null AR expression were indicated as AR-(Low/Neg). *P*-value for Fisher's exact test is indicated.

Based on our findings, we conjecture that *SPINK1* is one of the AR repressed genes, hence we next examined the expression of AR and other members of AR repressor complex (*NCOR1*, *NCOR2* and *NR1P1*) using TCGA-PRAD cohort, and the patients were sorted based on *SPINK1* high and low expression by employing quartile-based normalization<sup>38</sup>. Taken together, our findings show an inverse association between *SPINK1* expression and AR signaling in PCa patients, indicating that upregulation of *SPINK1* is owing to the loss of AR-mediated repression during PCa progression.

### ***AR antagonists trigger SPINK1 upregulation in PCa***

Since an inverse association between *SPINK1* expression and AR signaling was observed in three independent PCa cohorts (TCGA-PRAD, MSKCC and ours) (Fig. 1), we examined the role of AR signaling in the regulation of *SPINK1* using PCa cell lines, 22RV1 (endogenously *SPINK1*-positive) and androgen responsive VCaP cells (*TMPRSS2-ERG* fusion positive). Stimulating 22RV1 cells with synthetic androgen, R1881 (10nM), results in a significant decrease in expression of *SPINK1* with a concomitant increase in the expression of AR target gene, *KLK3* (Fig. 2a-c). Similarly, VCaP cells stimulated with R1881 (10nM) show a significant decline in the expression of *SPINK1* both at transcript and protein levels, while an increase in the expression of *KLK3* was noticed (Fig. 2d-f).



**Figure 2**

**Figure 2. Androgen signaling negatively regulates SPINK1 expression in prostate cancer.** (a) Immunoblot for SPINK1 in 22RV1 cells stimulated with R1881 (10nM) (top). QPCR data showing relative expression of SPINK1 and KLK3 in the same cells (bottom). (b) Immunostaining for SPINK1 and AR in 22RV1 cells stimulated with R1881 (10nM). (d) Same as (a), except VCaP cells were used. (e) Same as (b), except VCaP cells were used. (e) Immunoblot showing SPINK1 expression in VCaP cells treated with enzalutamide (top). QPCR data showing relative expression of SPINK1, KLK3 and ERG (bottom). (f) Immunostaining for SPINK1 and ERG using same cells as (e).

We also analyzed the publicly available datasets (GSE71797 and GSE51872), wherein 22RV1 and VCaP cells were stimulated with R1881 and dihydrotestosterone (DHT), respectively, which exhibits reduced expression of *SPINK1*, among the several previously known AR repressed genes, namely *DDC*, *OPRK1*, *NOV* and *SERPINI*<sup>39,40</sup> (Fig. 2g). Non-steroidal pharmacological inhibitors for AR, namely bicalutamide (Bic) and enzalutamide (Enza) have been widely used for the treatment of locally advanced non-metastatic and metastatic PCa<sup>33</sup>. Therefore, we determined the effect of these anti-androgens on SPINK1 expression in VCaP cells, and a treatment with Enza remarkably increased the *SPINK1* transcript (~4-fold) and protein levels, accompanied with reduced expression of androgen driven-genes namely *KLK3* and *ERG* (Fig. 2h-j). Taken together, our findings demonstrate that AR signaling negatively regulates SPINK1 expression and draws attention to AR antagonists mediated upregulation of SPINK1 in prostate cancer.

### *AR directs transcriptional repression of SPINK1 in PCa*

The role of AR has been extensively characterized both as a transcriptional activator as well as repressor<sup>39</sup>. To examine whether AR directly regulates *SPINK1* transcription we analyzed the presence of putative AR binding sites in the *SPINK1* promoter region, and scanned the region for the presence of androgen response elements (AREs) by employing publicly available transcription factor binding prediction software, JASPAR (<http://www.jaspar.genereg.net>) and MatInspector (<http://www.genomatix.de>). Several putative AREs within the ~5kb region upstream of transcription start site (TSS) of *SPINK1* were identified (Fig. 3a). Further, analysis of the publicly available Chromatin Immunoprecipitation-Sequencing (ChIP-Seq) dataset for AR binding in androgen stimulated VCaP cells (GSE8428) revealed another putative ARE on the *SPINK1* promoter (Fig. 3b)

**Figure 3**

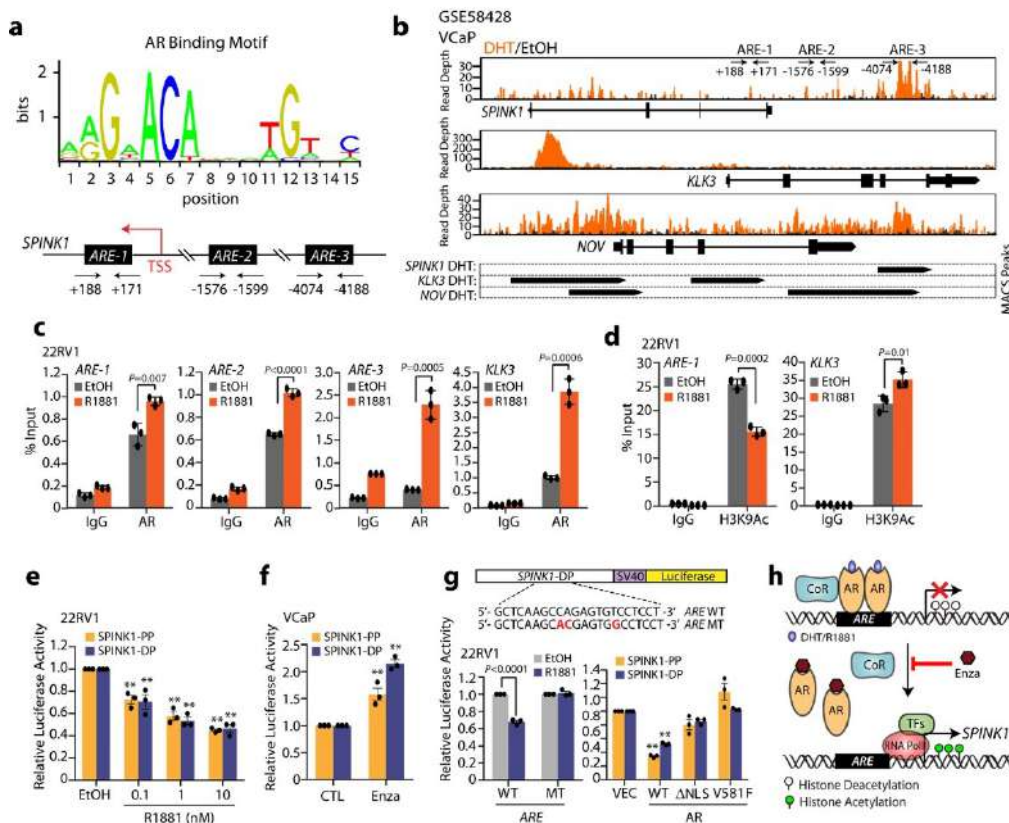


**Figure 3. AR directly binds to *SPINK1* promoter region and modulates its expression.** (a) Schema showing AR binding motif obtained from JASPAR database (top). Bottom panel showing genomic location for the AREs on the *SPINK1* promoter. (b) ChIP-Seq profiles indicating AR enrichment on the *SPINK1*, *KLK3* and *NOV* gene loci in androgen stimulated VCaP cells (GSE58428). Bottom panel indicates the MACS identified peaks for AR binding on the promoters of *SPINK1*, *KLK3* and *NOV*. (c) ChIP-qPCR data showing recruitment of AR on the *SPINK1* promoter upon R1881 (10nM) stimulation in 22RV1 cells. *KLK3* promoter was used as a positive control for the androgen stimulation experiment. (d) Same as in (c), except H3K9Ac (H3 lysine 9 acetylation) marks on the *SPINK1* and *KLK3* promoters. (e) Luciferase reporter activity of the proximal (*SPINK1*-PP) and distal *SPINK1* (*SPINK1*-DP) promoters in R1881(10nM) stimulated 22RV1 cells. (f) Same as in (e) except enzalutamide (10μM) treated VCaP cells were used. (g) Schematic showing luciferase reporter constructs with *SPINK1*-DP wild-type (WT) or mutated (MT) ARE sites (altered residues in red) (top). Luciferase reporter activity of *SPINK1*-DP WT or MT in R1881 stimulated (10nM) 22RV1 cells (bottom, left) and 22RV1 cells co-transfected with *SPINK1*-PP or *SPINK1*-DP and VEC, AR wildtype (WT) or AR mutants ( $\Delta$ NLS and V581F) constructs (bottom, right). (h) Illustration showing AR signaling mediated regulation of *SPINK1* in prostate cancer, wherein CoR (corepressor), TFs (transcription factors) and Enza (enzalutamide) is shown.

To confirm AR binding on the *SPINK1* promoter, we performed ChIP-quantitative PCR (ChIP-qPCR) for AR in R1881-stimulated 22RV1 cells, and a significant enrichment for AR-binding at three distinct sites (*ARE-1*, *ARE-2* and *ARE-3*) was observed (Fig. 3c). Moreover, a significant reduction in the enrichment of H3K9Ac activation marks on the *SPINK1* promoter was observed in R1881-stimulated 22RV1 cells, which further confirms its transcriptionally repressed-state (Fig. 3d). Conversely, enrichment of H3K9Ac marks on *KLK3* promoter indicates its transcriptionally active state (Fig. 3d).

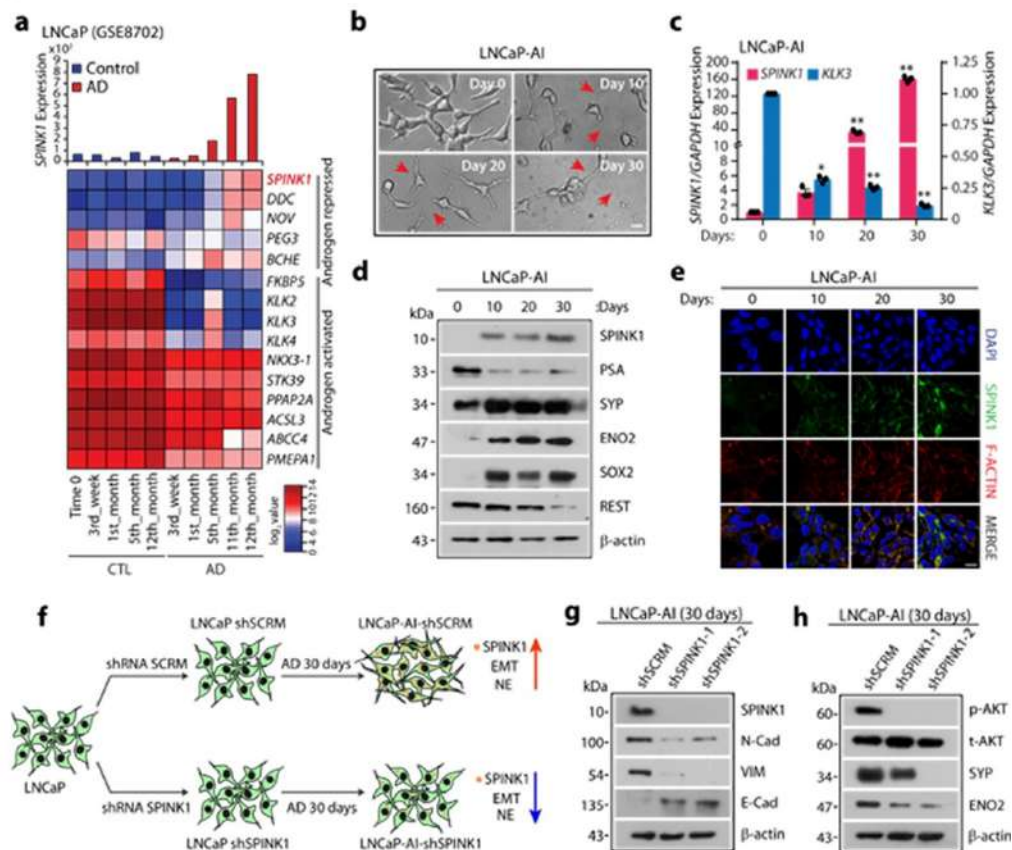
To further confirm the AR signaling-mediated transcriptional repression of *SPINK1*, we performed luciferase reporter assay using proximal (SPINK1-PP) and distal (SPINK1-DP) promoter regions of *SPINK1* in 22RV1 cells. A concentration dependent decrease in the luciferase activity was observed in 22RV1 cells transfected with SPINK1-PP and SPINK1-DP upon androgen stimulation (Fig. 3e). A significant increase in the luciferase activity of both the reporter constructs was observed upon Enza treatment (Fig. 3f). Further, we mutated ARE (ARE MT) in the SPINK1-DP construct and performed a luciferase assay, and as a result, no change in the luciferase activity was recorded in the 22RV1 cells transfected with mutant SPINK1-DP (Fig. 3g). Furthermore, 22RV1 cells transfected with wildtype or mutant AR ( $\Delta$ NLS and V581F) show significant decrease in the luciferase activity of both SPINK1-PP and SPINK1-DP with wildtype AR, while no change was observed with AR mutants (Fig. 3g). Together these findings indicated that the AR acts as a direct transcriptional repressor of *SPINK1*, and attenuating AR signaling using AR-antagonists relieve *SPINK1* transcriptional repression resulting in its upregulation (Fig. 3h).

### ***SPINK1 upregulation is associated with NE phenotype in PCa***

To understand the effect of long-term androgen deprivation on *SPINK1* expression, we analyzed publicly available gene expression dataset (GSE8702), wherein LNCaP cells (SPINK1-negative) were androgen deprived for 12 months. Remarkably, with prolonged androgen deprivation, a robust increase in the *SPINK1* expression was noticed (Fig. 4a). To confirm the association of SPINK1 upregulation with NE-transdifferentiation, LNCaP cells were cultured in androgen-deprived condition for 30 days (Fig. 4b). Consistent with previous report<sup>41</sup>, we observed a gradual change in the morphology of LNCaP cells, from an epithelial to a more NE-like phenotype (LNCaP-AI), an androgen-independent cell line, exhibiting neuron-like projections with a concomitant increase in the NEPC markers namely, SYP, CHGA, ENO2 and NCAM1, and a significant decrease in PSA and REST (Fig. 4b, d). Intriguingly, in LNCaP-AI and in long-term androgen-deprived C4-2 cells, a LNCaP derivative, show a remarkable increase in SPINK1 both at transcript and protein levels with concomitant drop in *KLK3* (Fig. 4c-e). Moreover, LNCaP-AI cells also show a significant increase in the expression of EMT (*NCAD*, *VIM* and *TWIST1*) and stemness markers (*SOX2*, *CD44* and *KIT*) (Fig. 4c & d).

To further confirm the role of SPINK1 in NE-transdifferentiation of LNCaP cells, we established stable *SPINK1*-silenced LNCaP cells (LNCaP-shSPINK1) and scrambled control (LNCaP-shSCRM) using lentivirus-based short-hairpin RNAs, and cultured them in androgen-deprived condition for 30 days (Fig. 4f). Phenotypically androgen-deprived LNCaP-AI-shSPINK1 show reduction in the length of neurite-like projections, indicating altered NE-transdifferentiation. Intriguingly, LNCaP-AI-shSPINK1 cells exhibit decrease in the markers for EMT (E-Cad, Vimentin and N-Cad) and NEPC (SYP and ENO2) as compared to LNCaP-AI-shSCRM cells (Fig. 4g-h), indicating the significance of SPINK1 in NE-transdifferentiation and cellular plasticity. Previous studies indicate the role of AKT signaling in advancement of PCa to poorly differentiated small cell prostate carcinoma<sup>42</sup>. Moreover, several studies have shown a critical role of SPINK1 in activating PI3K-AKT signaling cascade in multiple SPINK1-positive cancers<sup>43-45</sup>. In concordance to these reports, we also observed a remarkable decrease in AKT signaling in LNCaP-AI-shSPINK1 cells as compared to control cells (Fig. 4h). Collectively, our finding suggest that androgen-deprivation therapies may have an adverse effect, and the benefits must be weighed against treatment. Conclusively, we also show that elevated SPINK1 levels during NE-transdifferentiation strongly emphasizes the potential role of SPINK1 in governing stemness and cellular plasticity in prostate cancer.



**Figure 4**

**Figure 4. Androgen-deprivation upregulates SPINK1 in NE-transdifferentiated PCa cells.** (a) Bar graph showing *SPINK1* expression (top) and heatmap of AR-signaling associated genes including *SPINK1* in long-term androgen deprived (AD) LNCaP cells (GSE8702). (b) Representative phase-contrast images of androgen-deprived LNCaP cells (LNCaP-AI). Red arrow-heads indicate neurite outgrowth. (c) QPCR data showing relative expression of *SPINK1* and *KLK3* using same cells as (b). (d) Immunoblot assay for SPINK1, PSA, SYP, ENO2, SOX2 and REST using same cells as in (b). (e) Immunostaining for SPINK1 using same cells as in (b). (f) Schema describing generation of LNCaP-AI-shSPINK1 and LNCaP-AI-shSCRM cells by subjecting stable LNCaP-shSPINK1 and LNCaP-shSCRM cells to androgen deprivation (AD) for 30 days. (g) Immunoblot analysis for SPINK1, E-Cad, VIM and N-Cad expression using same cells as (f). (h) Same as in (g), except phosphor (p) and total (t) AKT, SYP and ENO2 expression.

### Expression of *SPINK1* is modulated by *SOX2* and *REST* in PCa

The role of SRY (sex determining region Y)-box 2 (*SOX2*) has been implicated in NE-differentiation and reprogramming/lineage plasticity in *RBI* and *TP53* deficient PCa<sup>46</sup>. Since, *SOX2* is a known androgen repressed gene<sup>47</sup>, we sought to examine *SOX2*-mediated regulation of *SPINK1*. We scanned the *SPINK1* promoter for *SOX2* binding motif using MatInspector, and identified three putative binding sites (*S1*, *S2* and *S3*) (Fig. 5a). To investigate that *SPINK1* up-regulation in LNCaP-AI cells is mediated through *SOX2* during NE-transdifferentiation, we examined *SOX2* occupancy on the *SPINK1* promoter using these cells and observed a remarkable enrichment of *SOX2* at three distinct binding sites (Fig. 5a). Similarly, 22RV1, an endogenously *SOX2* positive cell line, also exhibit a significant *SOX2* enrichment on the *SPINK1* promoter (Fig. 5b). Additionally, an increase in the occupancy of Pol-II was noticed on the *SPINK1* promoter in LNCaP-AI and 22RV1 cells (Fig. 5c, d), signifying its increased transcriptional activity. Furthermore, silencing *SOX2* in these cell lines result in a remarkable reduction in the *SPINK1* levels (Fig. 5e, f). Contrariwise, ectopic *SOX2* overexpression in LNCaP cells show a robust increase in the *SPINK1* expression (Fig. 5g). Finally, luciferase reporter assay also indicates a significant increase in the luciferase activity of *SPINK1*-DP

promoter in the SOX2 overexpressing LNCaP cells (Fig. 5h), thus reaffirming the SOX2-mediated positive transcriptional regulation of *SPINK1*.

**Figure 5**

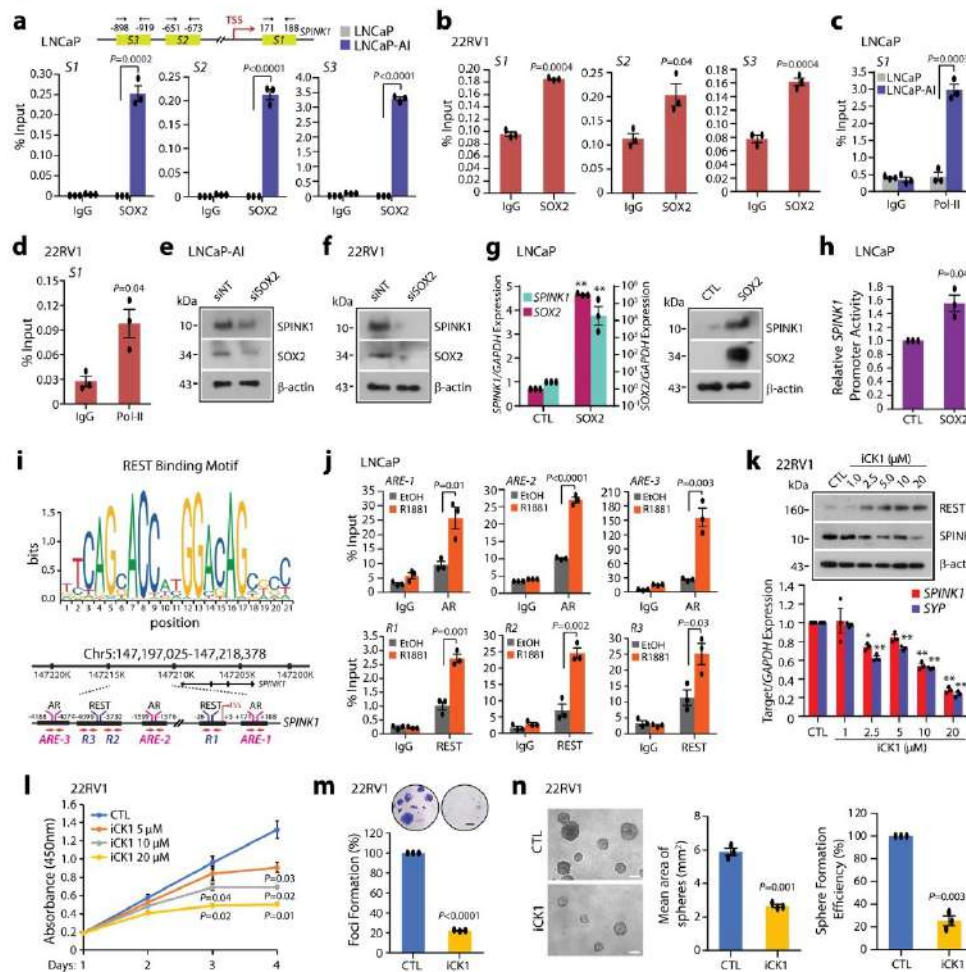


**Figure 5. Reprogramming factor SOX2 and AR transcriptional co-repressor REST modulate SPINK1 expression.** (a) Schematic showing SOX2 binding elements (S1, S2 and S3) on the *SPINK1* promoter (top). ChIP-qPCR data for SOX2 occupancy on the *SPINK1* promoter in wildtype LNCaP and LNCaP-AI cells (androgen-deprived for 15 days). (b) Same as in (a), except 22RV1 cells. (c) ChIP-qPCR data for RNA Pol-II binding on the *SPINK1* promoter using cells as (a). (d) Same as (c), except 22RV1 cells. (e) Immunoblot for SOX2 and SPINK1 in siRNA mediated *SOX2*-silenced LNCaP-AI and control cells. (f) Same as (e), except 22RV1 cells. (g) QPCR data showing relative expression of *SOX2* and *SPINK1* upon transient *SOX2* overexpression in LNCaP cells (left). Immunoblot for *SOX2* and *SPINK1* expression (right). (h) Luciferase reporter activity of the *SPINK1* distal-promoter (*SPINK1*-DP) using same cells as (g). (i) REST binding motif obtained from JASPAR (top). Genomic location for AR and REST binding on the *SPINK1* promoter (bottom). (j) ChIP-qPCR data showing AR and REST occupancy on the *SPINK1* promoter in R1881 stimulated (10nM) LNCaP cells. (k) Immunoblot for the REST and SPINK1 levels in 22RV1 cells treated with Casein Kinase 1 inhibitor (iCK1) as indicated (top). QPCR data for relative *SPINK1* and *SYP* expression (bottom). (l) Cell proliferation assay using 22RV1 cells treated with different concentrations of iCK1. (m) Foci formation assay using 22RV1 cells treated with iCK1 (20μM). Inset showing representative images depicting foci (Scale bar: 500μm). (n) Representative phase contrast microscopic images of 3D tumor spheroids using same cells as (m) (left). Bar plots depict mean area and efficiency of the sphere formation. Scale bar represents 1000μm.

Downregulation of REST, a transcriptional co-repressor of AR, plays a critical role in the progression of CRPC to NEPC<sup>48,49</sup>. Having established the role of AR signaling in *SPINK1* regulation and NE-transdifferentiation, we next examined the plausible association of *SPINK1* with REST and its other complex members in TCGA-PRAD and MSKCC cohorts. To investigate whether REST is acting as a transcriptional co-repressor of AR in *SPINK1* regulation, we examined *SPINK1* promoter for the REST binding motif within ~5 kb region of the TSS using MatInspector (Fig. 5i). A robust enrichment of AR at the AREs (*ARE-1*, *ARE-2* and *ARE-3*) along with REST recruitment at the three

distinct RE-1 sites (*R1*, *R2* and *R3*) adjacent to AREs on the *SPINK1* promoter was observed in androgen-stimulated LNCaP cells (Fig. 5j).

In hippocampal neurons, Casein Kinase 1 (CK1) is known to phosphorylate the non-canonical degron motifs in the C-terminal of REST, enabling its binding to the F-box protein E3 ubiquitin ligase SCF ( $\beta$ -TrCP). This, in turn, results in ubiquitin-mediated proteasomal degradation of REST<sup>50,51</sup>. Therefore, we restored REST levels in 22RV1 cells using CK1 inhibitor (iCK1, D4476), and observed a significant increase in the REST levels, with a concomitant decrease in the expression of *SPINK1*, *SYP* and other REST target genes (Fig. 5k). We next examined whether restoration of REST levels via iCK1 abrogates *SPINK1*-mediated oncogenic properties, by treating 22RV1 cells with a range of iCK1 concentrations. Intriguingly, a significant reduction in the cell proliferation and number of foci was observed in iCK1 treated 22RV1 cells (Fig. 5l, m). We also observed a significant reduction in the number and size of spheroids in the iCK1-treated 22RV1 cells using three-dimensional tumor spheroid assay (Fig. 5n). Collectively, we have shown the direct role of SOX2 in the transcriptional regulation of *SPINK1* in prostate cancer. We also establish that REST acts as a transcriptional corepressor of AR in modulating the *SPINK1* expression, thus a cease in AR signaling during NE-transdifferentiation results in *SPINK1* upregulation, and its overexpression positively associates with NE-like phenotype.

#### ***ADT upregulates SPINK1 and NE-markers in mice and PCa patients***

To investigate the impact of androgen ablation and mimic the effects of AR antagonists in CRPC, we used castrate-resistant tumors generated after orthotopic implantation of VCaP cells in immunodeficient (HSD/athymic nude– *Foxn1*<sup>nu</sup>) mice, administered with vehicle (Veh) or AR antagonists (Enza or ARN-509)<sup>52</sup>. Importantly, this study showed that androgen-deprivation in these mice resulted in reduced intra-tumoral androgen levels, leading to upregulation of androgen-repressed genes such as *NOV*. We next analyzed the RNA-seq data obtained from the Enza or ARN-509 treated mice (GSE95413), and a significant increase in the *SPINK1* levels, along with other NEPC (*SYP*, *CHGA* and *TUBB3*) and mesenchymal markers (*VIM*) was observed (Fig. 6a). Similar to transcriptomic data, a remarkable increase in the *SPINK1* expression accompanied with NE and mesenchymal markers was observed by IHC in tumors of AR-antagonists treated mice, thus reaffirming the association between *SPINK1* and NE-like phenotype (Fig. 6b, c).

Since *SPINK1* was found to be upregulated and associated with NE-markers in AR antagonists treated mouse xenografts, we next analyzed the RNA-seq data of the Beltran cohort<sup>53</sup> for *SPINK1* expression. Interestingly, 8 out of 36 NEPC patients show increased expression of *SPINK1*. Next, to validate the expression of *SPINK1*, AR and NE-markers in these patients, we selected NEPC cases on the basis of *SPINK1*-high and -low status, namely, WCM12, a patient who developed metastatic NEPC with liver metastases after treatment with ADT for metastatic prostate adenocarcinoma, who responded well to subsequent platinum-based chemotherapy<sup>54</sup>; WCM155, who also developed treatment-related NEPC after ADT with lung and liver metastases who responded well to the AURKA inhibitor alisertib on a clinical trial<sup>55</sup>; and WCM677, who developed metastatic NEPC after treatment with ADT and subsequent radium for CRPC, and harbored somatic alterations in *RB1*, *PTEN* and *BRCA2*<sup>53</sup>. Notably, similar to our *SPINK1* and AR IHC data in prostate adenocarcinoma patients (Fig. 1), WCM12 also showed positive staining for *SPINK1* and was negative for AR expression. WCM155 was developed as a patient-derived organoid which exhibited weak cytoplasmic staining for *SPINK1* and was negative for AR expression. Conversely, WCM677 showed negative staining for *SPINK1* expression and focal weak positive staining for AR (Fig. 6f). Collectively, our data demonstrate that androgen-deprivation using AR-antagonists leads to upregulation of *SPINK1*, which associates with NE-like features in our CRPC mice models. We also



provide an important proof-of-concept highlighting the significance of SPINK1 in context of NEPC progression. However, these findings need to be interrogated using larger cohort, and an in-depth mechanistic study underpinning the role of SPINK1 in NEPC would provide further clarity.

**Figure 6**

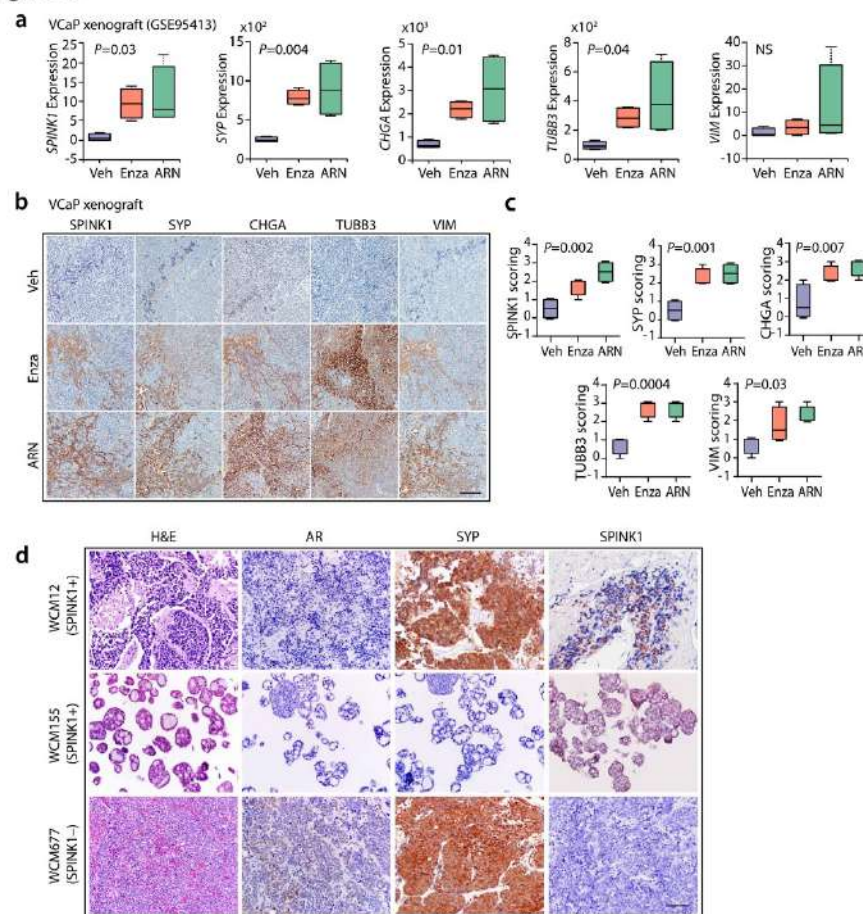


**Figure 6. ADT induced SPINK1 upregulation associates with NE-phenotype in mice and NEPC patients. (a)** Box plots depicting relative expression of *SPINK1*, *SYP*, *CHGA*, *TUBB3* and *VIM* transcripts (read counts) in VCaP tumors implanted orthotopically in orchiectomized mice and subjected to vehicle (n=4) or anti-androgens [enzalutamide (n=4) or ARN-509 (n=4)] treatment for 4 weeks (GSE95413). **(b)** Representative images of immunohistochemical staining for the same markers shown in (a) using VCaP xenograft tumors as described in (a). Scale bar represents 100 $\mu$ m. **(c)** Box plots depicting quantification of the immunohistochemical staining in VCaP xenografts for the markers shown in (b). **(d)** Representative images showing H&E staining (200x magnification) and immunostaining (200x magnification) for AR, synaptophysin, and SPINK1 in tumor specimens obtained from NEPC patients, namely WCM12, WCM155 (an organoid), and WCM677. Scale bar represents 100 $\mu$ m.

Importantly, our data revealed that targeting the ubiquitin-dependent REST degradation using iCK1 results in reduced expression of SPINK1 and REST targets, subsequently leading to decrease in oncogenic properties. Collectively, our findings suggest that AR and REST modulate the expression of *SPINK1*, thus stabilizing REST levels may be an alternate therapeutic strategy for controlling SPINK1-mediated oncogenicity and NEPC progression. Ablation of androgen signaling has been implicated in upregulation of several EMT markers, a phenotype often associated with PCa metastases<sup>31</sup>. Further, a bidirectional negative-feedback loop between AR and ZEB1 has been established, which drives EMT and stem cell-like features upon androgen deprivation in LuCaP35 tumor explants<sup>31</sup>. Recently, we have shown that SPINK1 expression positively correlates with EZH2, a member of Polycomb repressive complex 2, known to induce pluripotency and stemness<sup>56</sup>. Furthermore, SOX2 has been implicated as a key regulator in governing pluripotency and drives NE-transdifferentiation<sup>46</sup>.



## Impact of the research in the advancement of knowledge or benefit to mankind

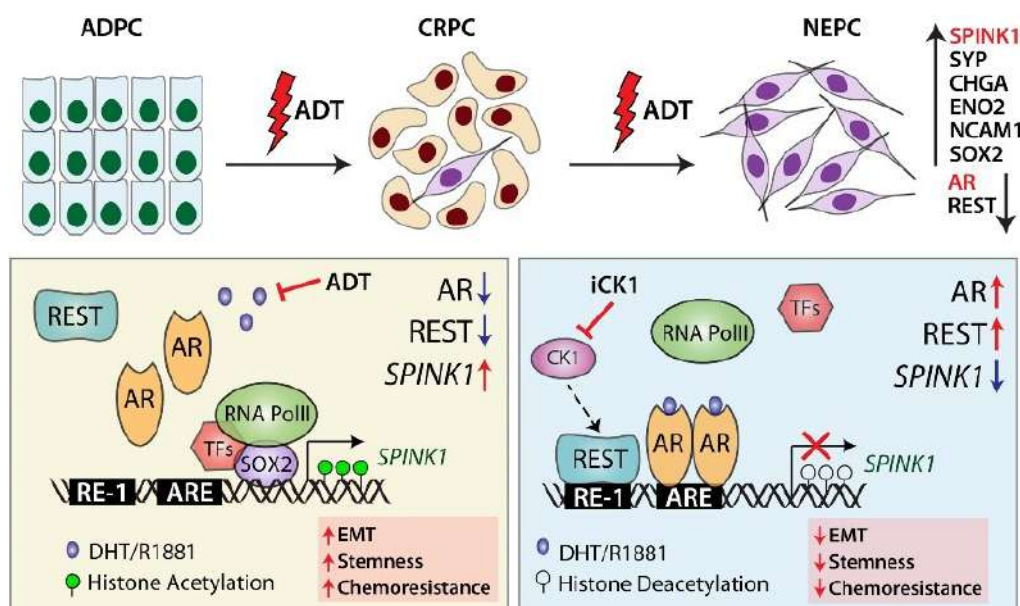


**Figure 7. Androgen receptor and its transcriptional co-repressor REST modulate *SPINK1* expression.** Schematic showing androgen deprivation therapy (ADT) induced progression of prostate adenocarcinoma (ADPC) to neuroendocrine prostate cancer (NEPC) (top panel). ADT using AR-antagonists relieve AR-REST mediated transcriptional repression of *SPINK1*, and subsequently, SOX2 gets recruited on the *SPINK1* promoter resulting in its upregulation (left box). Additionally, Casein kinase 1 inhibitor (iCK1) restores REST levels causing downregulation of *SPINK1*, leading to reduced stemness and cellular plasticity (right box).

This seminal discovery shifted the paradigm about androgen deprivation therapy (ADT), wherein anti-androgen drugs (Enzalutamide or XTANDI) commonly used for treating advanced stage prostate cancer patients is actually counterproductive in the long-term. We demonstrated that AR and its corepressor REST negatively regulates the *SPINK1* expression, and long-term androgen deprivation or treatment with AR antagonists in PCa cell lines, mice xenograft models as well as PCa patients result in elevated levels of *SPINK1*, accompanied with transdifferentiation of prostate cancer cells to an aggressive subtype with neuroendocrine (NE)-like features. Also, silencing *SPINK1* in NE-transdifferentiated PCa cells exhibit remarkable decrease in the expression of NEPC markers as well as cellular plasticity. ***Most importantly, we showed that pharmacological inhibition of Casein Kinase-1 stabilizes REST levels, which in cooperation with AR represses SPINK1 transcription, and impedes SPINK1-mediated oncogenesis. This study provides an explanation for the paradoxical clinical-outcomes after ADT, possibly due to SPINK1 upregulation, and offers an alternative treatment strategy.*** Conclusively, our findings emphasize that administering PCa patients with AR targeted therapies may result in increased *SPINK1* levels accompanied by upregulation of NE markers, potentially promoting the development of treatment-related NEPC. Although, androgen ablation therapy is a well-established and highly effective treatment for PCa patients, resistance ultimately ensues. Understanding resistance mechanisms to ADT and subsequent AR therapies will eventually lead to more effective treatment strategies to improve outcomes for patients developing AR independent disease.

## References

- 1 Panganiban, G. & Rubenstein, J. L. Developmental functions of the Distal-less/Dlx homeobox genes. *Development* **129**, 4371-4386 (2002).
- 2 Abate-Shen, C. Deregulated homeobox gene expression in cancer: cause or consequence? *Nature reviews. Cancer* **2**, 777-785, doi:10.1038/nrc907 (2002).
- 3 Chiba, S. *et al.* Homeoprotein DLX-1 interacts with Smad4 and blocks a signaling pathway from activin A in hematopoietic cells. *Proceedings of the National Academy of Sciences of the United States of America* **100**, 15577-15582, doi:10.1073/pnas.2536757100 (2003).
- 4 Liang, M. *et al.* DLX1, a binding protein of beta-catenin, promoted the growth and migration of prostate cancer cells. *Experimental cell research* **363**, 26-32 (2018).
- 5 Van Neste, L. *et al.* Detection of high-grade prostate cancer using a urinary molecular biomarker-based risk score. *European urology* **70**, 740-748 (2016).
- 6 Li, T. *et al.* ALDH1A1 is a marker for malignant prostate stem cells and predictor of prostate cancer patients' outcome. *Laboratory investigation* **90**, 234 (2010).
- 7 Tomita, H., Tanaka, K., Tanaka, T. & Hara, A. Aldehyde dehydrogenase 1A1 in stem cells and cancer. *Oncotarget* **7**, 11018 (2016).
- 8 Abel, E. V. *et al.* HNF1A is a novel oncogene that regulates human pancreatic cancer stem cell properties. *Elife* **7**, e33947 (2018).
- 9 Lézot, F. *et al.* Dlx homeobox gene family expression in osteoclasts. *Journal of cellular physiology* **223**, 779-787 (2010).
- 10 Wang, M., Xia, F., Wei, Y. & Wei, X. Molecular mechanisms and clinical management of cancer bone metastasis. *Bone Research* **8**, 1-20 (2020).
- 11 Abida, W. *et al.* Genomic correlates of clinical outcome in advanced prostate cancer. *Proceedings of the National Academy of Sciences* **116**, 11428-11436 (2019).
- 12 Bose, R. *et al.* ERF mutations reveal a balance of ETS factors controlling prostate oncogenesis. *Nature* **546**, 671-675 (2017).
- 13 Sandoval, G. J. *et al.* Binding of TMPRSS2-ERG to BAF chromatin remodeling complexes mediates prostate oncogenesis. *Molecular cell* **71**, 554-566. e557 (2018).
- 14 Rickman, D. S. *et al.* Oncogene-mediated alterations in chromatin conformation. *Proceedings of the National Academy of Sciences* **109**, 9083-9088 (2012).
- 15 Chng, K. R. *et al.* A transcriptional repressor co-regulatory network governing androgen response in prostate cancers. *The EMBO journal* **31**, 2810-2823 (2012).
- 16 Pomerantz, M. M. *et al.* The androgen receptor cistrome is extensively reprogrammed in human prostate tumorigenesis. *Nature genetics* **47**, 1346 (2015).
- 17 Jin, H.-J., Zhao, J. C., Wu, L., Kim, J. & Yu, J. Cooperativity and equilibrium with FOXA1 define the androgen receptor transcriptional program. *Nature communications* **5**, 3972 (2014).
- 18 Yu, J. *et al.* An integrated network of androgen receptor, polycomb, and TMPRSS2-ERG gene fusions in prostate cancer progression. *Cancer cell* **17**, 443-454 (2010).
- 19 Zhang, Z. *et al.* An AR-ERG transcriptional signature defined by long-range chromatin interactomes in prostate cancer cells. *Genome research* **29**, 223-235 (2019).
- 20 Ramanand, S. G. *et al.* The landscape of RNA polymerase II associated chromatin interactions in prostate cancer. *The Journal of Clinical Investigation* (2020).
- 21 He, Y. *et al.* Androgen receptor splice variants bind to constitutively open chromatin and promote abiraterone-resistant growth of prostate cancer. *Nucleic acids research* **46**, 1895-1911 (2018).
- 22 Asangani, I. A. *et al.* Therapeutic targeting of BET bromodomain proteins in castration-resistant prostate cancer. *Nature* **510**, 278 (2014).
- 23 Aggarwal, R. R. *et al.* A Phase Ib/IIa Study of the Pan-BET Inhibitor ZEN-3694 in Combination with Enzalutamide in Patients with Metastatic Castration-resistant Prostate Cancer. *Clinical Cancer Research* **26**, 5338-5347 (2020).
- 24 Asangani, I. A. *et al.* BET bromodomain inhibitors enhance efficacy and disrupt resistance to AR antagonists in the treatment of prostate cancer. *Molecular Cancer Research* **14**, 324-331 (2016).
- 25 Stathis, A. & Bertonni, F. BET proteins as targets for anticancer treatment. *Cancer discovery* **8**, 24-36 (2018).
- 26 Tomlins, S. A. *et al.* The role of SPINK1 in ETS rearrangement-negative prostate cancers. *Cancer cell* **13**, 519-528, doi:10.1016/j.ccr.2008.04.016 (2008).
- 27 Faisal, F. A. *et al.* SPINK1 expression is enriched in African American prostate cancer but is not associated with altered immune infiltration or oncologic outcomes post-prostatectomy. *Prostate cancer and prostatic diseases*, doi:10.1038/s41391-019-0139-0 (2019).
- 28 Flavin, R. J. *et al.* SPINK1 protein expression and prostate cancer progression. *Clinical Cancer Research*, clincanres. 1341.2013 (2014).
- 29 Leinonen, K. A. *et al.* Association of SPINK1 expression and TMPRSS2:ERG fusion with prognosis in endocrine-treated prostate cancer. *Clin Cancer Res* **16**, 2845-2851, doi:10.1158/1078-0432.CCR-09-2505 (2010).

- 30 Johnson, M. H. *et al.* SPINK1 Defines a Molecular Subtype of Prostate Cancer in Men with More Rapid Progression in an at Risk, Natural History Radical Prostatectomy Cohort. *J Urol* **196**, 1436-1444, doi:10.1016/j.juro.2016.05.092 (2016).
- 31 Sun, Y. *et al.* Androgen deprivation causes epithelial-mesenchymal transition in the prostate: implications for androgen-deprivation therapy. *Cancer research* **72**, 527-536, doi:10.1158/0008-5472.CAN-11-3004 (2012).
- 32 Karantanos, T., Corn, P. G. & Thompson, T. C. Prostate cancer progression after androgen deprivation therapy: mechanisms of castrate resistance and novel therapeutic approaches. *Oncogene* **32**, 5501-5511, doi:10.1038/ncr.2013.206 (2013).
- 33 Scher, H. I. *et al.* Antitumour activity of MDV3100 in castration-resistant prostate cancer: a phase 1-2 study. *Lancet* **375**, 1437-1446, doi:10.1016/S0140-6736(10)60172-9 (2010).
- 34 Clegg, N. J. *et al.* ARN-509: a novel antiandrogen for prostate cancer treatment. *Cancer research* **72**, 1494-1503, doi:10.1158/0008-5472.CAN-11-3948 (2012).
- 35 de Bono, J. S. *et al.* Abiraterone and increased survival in metastatic prostate cancer. *The New England journal of medicine* **364**, 1995-2005, doi:10.1056/NEJMoa1014618 (2011).
- 36 Rickman, D. S., Beltran, H., Demichelis, F. & Rubin, M. A. Biology and evolution of poorly differentiated neuroendocrine tumors. *Nature medicine* **23**, 664 (2017).
- 37 Beltran, H. *et al.* Aggressive variants of castration-resistant prostate cancer. *Clinical cancer research : an official journal of the American Association for Cancer Research* **20**, 2846-2850, doi:10.1158/1078-0432.CCR-13-3309 (2014).
- 38 Dillies, M. A. *et al.* A comprehensive evaluation of normalization methods for Illumina high-throughput RNA sequencing data analysis. *Briefings in bioinformatics* **14**, 671-683, doi:10.1093/bib/bbs046 (2013).
- 39 Zhao, J. C. *et al.* Cooperation between Polycomb and androgen receptor during oncogenic transformation. *Genome Res* **22**, 322-331, doi:10.1101/gr.131508.111 (2012).
- 40 Wu, L. *et al.* CCN3/NOV gene expression in human prostate cancer is directly suppressed by the androgen receptor. *Oncogene* **33**, 504-513, doi:10.1038/ncr.2012.602 (2014).
- 41 Yuan, T. C. *et al.* Androgen deprivation induces human prostate epithelial neuroendocrine differentiation of androgen-sensitive LNCaP cells. *Endocr Relat Cancer* **13**, 151-167, doi:10.1677/erc.1.01043 (2006).
- 42 Park, J. W. *et al.* Reprogramming normal human epithelial tissues to a common, lethal neuroendocrine cancer lineage. *Science* **362**, 91-95, doi:10.1126/science.1257499 (2018).
- 43 Ateeq, B. *et al.* Therapeutic targeting of SPINK1-positive prostate cancer. *Science translational medicine* **3**, 72ra17, doi:10.1126/scitranslmed.3001498 (2011).
- 44 Tiwari, R. *et al.* SPINK1 promotes colorectal cancer progression by downregulating Metallothioneins expression. *Oncogenesis* **4**, e162, doi:10.1038/ncs.2015.23 (2015).
- 45 Chen, F. *et al.* Targeting SPINK1 in the damaged tumour microenvironment alleviates therapeutic resistance. *Nature Communications* **9**, 4315, doi:10.1038/s41467-018-06860-4 (2018).
- 46 Mu, P. *et al.* SOX2 promotes lineage plasticity and antiandrogen resistance in TP53- and RB1-deficient prostate cancer. *Science* **355**, 84-88 (2017).
- 47 Kregel, S. *et al.* Sox2 is an androgen receptor-repressed gene that promotes castration-resistant prostate cancer. *PloS one* **8**, e53701 (2013).
- 48 Lapuk, A. V. *et al.* From sequence to molecular pathology, and a mechanism driving the neuroendocrine phenotype in prostate cancer. *J Pathol* **227**, 286-297, doi:10.1002/path.4047 (2012).
- 49 Svensson, C. *et al.* REST mediates androgen receptor actions on gene repression and predicts early recurrence of prostate cancer. *Nucleic acids research* **42**, 999-1015, doi:10.1093/nar/gkt921 (2014).
- 50 Kaneko, N., Hwang, J. Y., Gertner, M., Pontarelli, F. & Zukin, R. S. Casein kinase 1 suppresses activation of REST in insulated hippocampal neurons and halts ischemia-induced neuronal death. *J Neurosci* **34**, 6030-6039, doi:10.1523/JNEUROSCI.4045-13.2014 (2014).
- 51 Westbrook, T. F. *et al.* SCFbeta-TRCP controls oncogenic transformation and neural differentiation through REST degradation. *Nature* **452**, 370-374, doi:10.1038/nature06780 (2008).
- 52 Knuutila, M. *et al.* Antiandrogens Reduce Intratumoral Androgen Concentrations and Induce Androgen Receptor Expression in Castration-Resistant Prostate Cancer Xenografts. *Am J Pathol* **188**, 216-228, doi:10.1016/j.ajpath.2017.08.036 (2018).
- 53 Beltran, H. *et al.* Divergent clonal evolution of castration-resistant neuroendocrine prostate cancer. *Nature medicine* **22**, 298 (2016).
- 54 Beltran, H. *et al.* Whole-Exome Sequencing of Metastatic Cancer and Biomarkers of Treatment Response. *JAMA oncology* **1**, 466-474, doi:10.1001/jamaoncol.2015.1313 (2015).
- 55 Beltran, H. *et al.* A Phase II Trial of the Aurora Kinase A Inhibitor Alisertib for Patients with Castration-resistant and Neuroendocrine Prostate Cancer: Efficacy and Biomarkers. *Clin Cancer Res* **25**, 43-51, doi:10.1158/1078-0432.CCR-18-1912 (2019).
- 56 Bhatia, V. *et al.* Epigenetic Silencing of miRNA-338-5p and miRNA-421 Drives SPINK1-Positive Prostate Cancer. *Clinical cancer research : an official journal of the American Association for Cancer Research* **25**, 2755-2768, doi:10.1158/1078-0432.CCR-18-3230 (2019).